MODELING AND NUMERICAL INVESTIGATION OF HOT GAS DEFROST ON A FINNED TUBE EVAPORATOR USING COMPUTATIONAL FLUID DYNAMICS

A Thesis

presented to

the Faculty of California Polytechnic State University,

San Luis Obispo

In Partial Fulfillment

of the Requirements for the Degree

Master of Science in Mechanical Engineering

by

Oai The Ha

October, 2010

COMMITTEE MEMBERSHIP

TITLE:	Modeling and Numerical Investigation of Hot Gas Defrost on a Finned Tube Evaporator Using Computational Fluid Dynamics
AUTHOR:	Oai The Ha
DATE SUBMITTED:	October 2010
COMMITTEE CHAIR:	Jesse Maddren, Professor
COMMITTEE MEMBER:	Kim Shollenberger, Professor
COMMITTEE MEMBER:	Glen Thorncroft, Associate Chair

ABSTRACT

Modeling and Numerical Investigation of Hot Gas Defrost on a Finned Tube Evaporator Using Computational Fluid Dynamics.

Oai The Ha

Defrosting in the refrigeration industry is used to remove the frost layer accumulated on the evaporators after a period of running time. It is one way to improve the energy efficiency of refrigeration systems. There are many studies about the defrosting process but none of them use computational fluid dynamics (CFD) simulation. The purpose of this thesis is (1) to develop a defrost model using the commercial CFD solver FLUENT to simulate numerically the melting of frost coupled with the heat and mass transfer taking place during defrosting, and (2) to investigate the thermal response of the evaporator and the defrost time for different hot gas temperatures and frost densities.

A 3D geometry of a finned tube evaporator is developed and meshed using Gambit 2.4.6, while numerical computations were conducted using FLUENT 12.1. The solidification and melting model is used to simulate the melting of frost and the Volume of Fluid (VOF) model is used to render the surface between the frost and melted frost during defrosting. A user-defined-function in C programming language was written to model the frost evaporation and sublimation taking place on the free surface between frost and air. The model was run under different hot gas temperatures and frost densities and the results were analyzed to show the effects of these parameters on defrosting time, input energy and stored energy in the metal mass of the evaporator. The analyses demonstrate that an optimal hot gas temperature can be identified so that the defrosting process takes place at the shortest possible melting time and with the lowest possible input energy.

Keywords: hot gas defrost, phase change, frost melting, VOF, CFD simulation

ACKNOWLEDGMENTS

I would like to acknowledge the advice and guidance of Dr. Jesse Maddren, thesis advisor. I also thank the members of my graduate committee for their guidance and suggestions, especially Dr. Kim Shollenberger for all her advice.

I also thank Mr. Larry Coolidge for his technical support at the Bently Pressurized Bearings CAD Lab.

I acknowledge my friends, Vu Huy Chau and Karen My Anh Tran, for their encouragements and their kind support.

I dedicate this thesis to my mother and my late father who always encouraged me to achieve whatever goals I set for myself.

TABLE OF CONTENTS

TABLE OF CONTENTS (cont'd)

TABLE OF CONTENTS (cont'd)

LIST OF TABLES

LIST OF FIGURES

NOMENCLATURE

Name	Description
A	Air-frost interface area, [m^2]
$A_{tube\text{-}heat}$	Area of tube-heat surface, [m^2]
c_p	Specific heat, [J/kg-K]
D_{w2a}	Mass diffusivity of the water in air, [m^2/s]
Gr	Grashof number
h	Sensible heat enthalpy, [J/kg]
h_m	Mass transfer coefficient, [m/s]
h_f	Heat transfer coefficient, [W/m^2-K]
H	Enthalpy, [J/kg]
k	Thermal conductivity, [W/m-k]
L	Characteristic length, [m]
L_{evap}	Latent heat of evaporation, [J/kg]
L_{fus}	Latent heat of fusion, [J/kg]
L_{sub}	Latent heat of sublimation, [J/kg]
Nu	Nusselt number
P	Pressure, [Pa]
Pr	Prandtl number
q	Heat flux, [W]
Q	Heat energy, [J]
Ra	Raleigh number

S	Momentum source/sink term, [N/m^3]
S_n	Energy source/sink term, [W/m^3]
Sc	Schmidt number
Sh	Sherwood number
T	Temperature, [K]
V	Velocity, [m/s]

Greek symbols

α	Volume fraction
β	Thermal Expansion Coefficient, [K^{-1}]
λ	Liquid fraction
v	Kinematic viscosity, [m^2/s]
ρ	Density, [kg/m^3]
ρ_M	Average density of air mixture, [kg/m^3]

Subscripts

a	Air
am	Ambient
$evap$	Evaporation
L	Characteristic length
liq	Liquidus
ref	Reference

NOMENCLATURE (cont'd)

sat	Saturated
sol	Solidus
sub	Sublimation
tube	Tube
w	Water

Chapter 1. INTRODUCTION

1.1 Defrost Introduction

Frost accumulated on finned tube refrigeration equipment (referred to as an evaporator or heat exchanger) results in an increase in the heat transfer resistance as well as an increase in pressure drop across the finned tubes. Frost blocks the airflow passages, leading to reductions in the coefficient of performance (COP) and the system capacity. Frequent defrosting can restore the COP of the refrigeration system and reduce the overall energy consumption.

Defrosting is a complex and transient process that involves both heat and mass transfer. During the hot gas defrost, the metal tube and fin conduct thermal energy from hot gas inside the tube, thawing the bottom layer of frost in contact with the external tube and fin surfaces. The melted water permeates into the frost layer by capillary action or gravity, and then warms the frost surrounding it. Some of melted water evaporates into the air but most of melted water drains down under gravity to the drain pan. If the temperature in the frost layer is lower than the fusion temperature, refreezing of the permeating water can occur. The frost does not melt uniformly throughout the heat exchanger. Depending on evaporator geometry, surrounding air temperature, metal roughness, and relative position of the tube in the evaporator, frost can be melted completely at some spots, and only partially at other parts of the evaporator.

There are five defrost methods currently used in the commercial refrigeration industry [1]:

1) Natural defrost: In this method, the condensing unit is turned off while the evaporator defrosts. Since the energy required for defrosting is taken from the surrounding air, this method takes a lot of time.
2) Hot gas defrost: In this method, the hot gas is rerouted from the compressor discharge through the outlet of the evaporator. Heat is added directly to the evaporator coils without depending on an external heat source. The hot gas defrost is quick and consumes less energy, although the extra valve and piping incurs extra initial cost.
3) Electric defrost: Electric power is used to heat accumulated frost externally. This method requires special evaporators made for that purpose only.
4) Water defrost**:** In this method**,** water is sprayed directly on the evaporators while the compressor is turned off. The sensible heat of the water is used as a heat source to thaw the accumulated frost layer externally. The drains are usually electrically heated for this system. The water is circulated by a pump controlled by a time clock. The timer stops the compressor during defrost and energizes the electric drain heater.
5) Other external heat source: Other methods are possible such as using a secondary fluid, like glycol, as a heat transfer vehicle. This secondary fluid is pre-heated by electricity, steam, or other methods to add sufficient quantities of energy to obtain rapid defrosting. The heat is applied by circulating the secondary fluid in an inner tube of the evaporator coiling, thereby accomplishing a rapid defrost with a minimum of heat lost to the surrounding air.

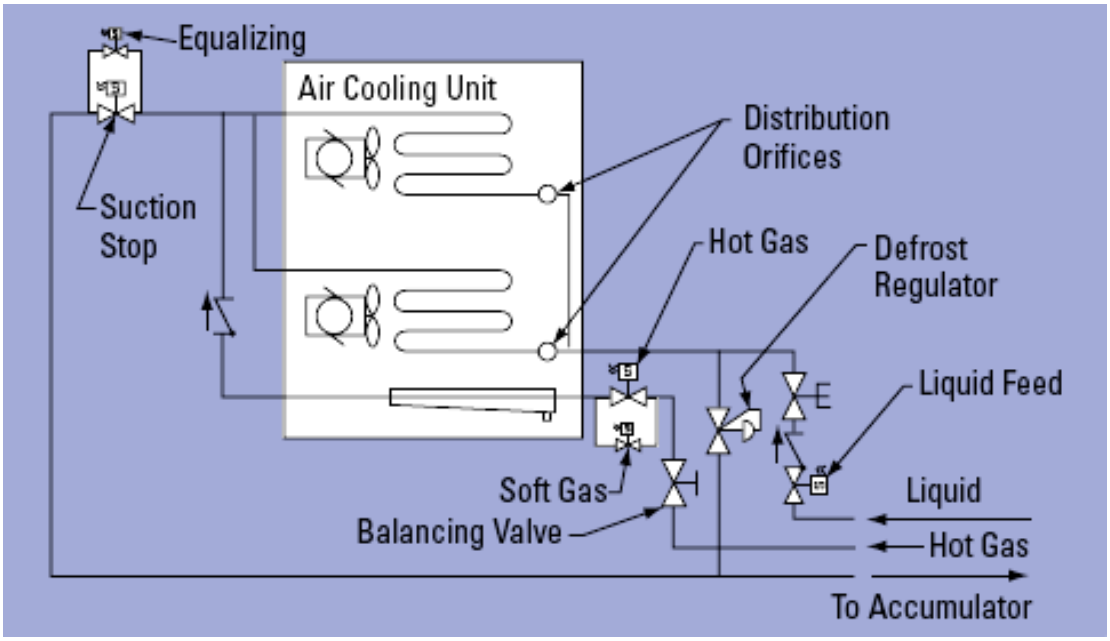

Figure 1. Basic piping arrangement with hos gas defrost

(from Parker Hannifin Corporation Bulletin, January 2007) [2]

Of the five defrost methods, hot gas defrost is the most common one due to the simplicity and reduced cost. Figure 1 shows a typical evaporator piping arrangement with hot gas defrost. The sequences of events that occur during hot gas defrost are as follows [2]:

1. Refrigeration Phase: Saturated liquid refrigerant flows through a liquid feed valve, into the evaporator. Heat is absorbed and some (or all) of the refrigerant vaporizes. The refrigerant exits through the open suction stop valve and flows to an accumulator.

2. Pump Out Phase: The liquid feed valve is closed. The fans continue to run, and liquid inside the coil vaporizes and exits through the suction stop valve.

Removing liquid from the coil during this phase allows heat from the hot gas to be applied directly to the frost instead of being wasted on warming liquid refrigerant. In addition, removal of the cold liquid prevents damaging pressure shocks. At the end of the pump out phase, the fans are shut down and the suction stop valve is closed.

3. Soft Gas Phase: Especially on low temperature liquid recirculation systems, a small solenoid valve should be installed in parallel with the larger hot gas valve. This smaller valve gradually introduces hot gas to the coil. Opening this valve first further reduces the likelihood of damaging pressure shocks. At the conclusion of this phase, the soft gas valve is closed.

4. Hot Gas Phase: The hot gas solenoid is opened and hot gas now flows more quickly through the drain pan, warming it, and then into the coil. The gas begins condensing as it gives up heat to melt the frost, and the pressure inside the coil rises sufficiently for control by the defrost regulator. The condensed refrigerant flows through the regulator and is routed to an accumulator or protected suction line. Hot gas continues to flow into the evaporator until either a pre-set time limit is reached, or until a sensor determines the defrost is complete and the hot gas valve is closed.

5. Equalization Phase: Especially on low temperature liquid re-circulating units, the pressure inside the coil is permitted to decrease slowly by opening a small equalizing valve that is installed in parallel with the larger main suction stop valve. The equalization phase reduces or eliminates system disruptions, which would occur if warm refrigerant were released quickly into the suction piping.

6. Fan Delay Phase: At the conclusion of the equalization phase, the equalizing valve is closed. The suction stop and liquid feed valves are opened. The fan is not yet energized. Instead, the coil temperature is allowed to drop, freezing any water droplets that might remain on the coil surface after the hot gas phase, thereby preventing the possibility of blowing water droplets off the coil into the refrigerated space.

7. Resume Refrigeration: After the fan delay has elapsed, the fan is energized. The refrigeration phase continues until the next defrost cycle is initiated.

1.2 Review of Existing Defrost Models

There are many investigators who have studied hot gas defrost. Krakow et al. [3, 4] introduced a numerical model in which the hot gas defrosting process is subdivided into four stages: preheating, melting, vaporizing, and dry heating in accordance with the coil surface conditions: frosted, slushy, wet and dry. Each element of a coil may pass through three or four stages. The model predicts that the major portion of the energy goes towards melting frost and vaporizing water. Al-Mutawa et al. [5] developed an analytical model for hot gas defrosting of a cylindrical coil cooler (i.e., an evaporator coil with no fins). In their model, a moving boundary technique is used and the defrost process was divided into two stages, pre-melting and melting stages. The experimental work conducted in a companion investigation documented the energy penalty associated with using hot-gas defrosting in industrial freezers. This penalty is realized by the large amount of the defrost heat input being transferred to the refrigerated space due to the evaporation of the melt and sublimation of frost (latent heat), as compared to the smaller

amount that is utilized to melt the frost. Part of this penalty is also attributed to the residual energy that goes into the refrigerant during the defrosting process. Hoffenbecker [6] and Hoffenbecker et al. [7] developed a numerical model to simulate the hot gas defrost process on industrial evaporator coils by discretizing the computational domain into concentric ring elements. The simulations were conducted by using Engineering Equation Solver (EES) software with different frost thicknesses, densities and hot gas temperature settings. Frost is assumed to be attached to the fin surface only, leaving the tube surface exposed to the air. In practice, when the frost melts, the resulting water drains and the node formerly occupied by frost is replaced by air, which has a much lower density. However, the model assumes that the density of the node is constant regardless whether it is occupied by air or by frost. This assumption results in the overestimation of the mass specific heat product when the node should be air. Despite these limitations, their model's energy distribution was validated against experimental data.

Dopazo et al. [8] divided the whole defrosting process into six consecutive stages: preheating, tube frost melting start, fin frost melting start, air presence, tube-fin water film and dry heating. Different governing equations are applied for each stage depending on the nature and physical phenomena occurring during the stage. The evaporator was modeled as one tube divided into smaller control volumes, from the hot gas inlet to the hot gas outlet. Each control volume was composed from a tube with a length equal to the distance between two fins and the corresponding portion of fin. A computer model was developed using Visual Basic. The results included: time required to defrost, and the

instantaneous fin and tube temperature distribution. These results were compared with both experimental data and Hoffenbecker's model data [6] with good agreement.

Dansilasirithavorn [9] applied the model developed by Hoffenbecker et al. [7] with the temperature finite difference method on EES software to determine the temperatures of an evaporator coil during defrost. Another model was also developed to calculate the pressure drop on the air side of the coil with and without frost. The results were intended to detect frost formation and initiate the defrost process. The model results were compared with data obtained at an operating refrigerated warehouse. The results indicated there was little frost formation while data was acquired and so comparisons with the model results were limited.

1.3 Computational Tool

Defrosting is a complex and transient process that involves multiple simultaneous physical phenomena. The current study uses commercially available Computational Fluid Dynamics (CFD) software to solve this problem numerically. CFD discretizes the spatial domain and solves the governing equations for mass, momentum, and energy for each finite volume. CFD software helps users build virtual models to simulate flows of gases and liquids, with heat and mass transfer without building a physical model, which in many cases can be complicated, expensive, and time consuming.

The current study uses FLUENT (by ANSYS), a commercially available software package that uses the finite-volume method. Gambit, a commercially available preprocessor also by ANSYS, was also used to develop the mesh for all models.

1.4 FLUENT Models and Limitations

1.4.1 FLUENT Models

FLUENT (version 12.1) offers a wide array of physical models that can be applied to a wide array of industries. All modes of heat transfer can be modeled, including conjugate heat transfer problems. Incompressible, compressible, laminar and turbulent fluid flow problems can also be modeled. In addition, special applications such as porous media and multiphase flows can also be considered. Some of the physical phenomena involved in defrosting are reviewed below [10-12]:

• Heat Transfer: Heat transfer can be significant for all three modes: conduction, convection, and radiation. FLUENT allows users to include heat transfer within the fluid and/or solid regions in their models.

• Solidification and Melting: FLUENT can be used to solve fluid flow problems involving solidification and/or melting taking place at one temperature (e.g., in pure metals) or over a range of temperatures (e.g., in binary alloys). Instead of tracking the liquid-solid front explicitly, FLUENT uses an enthalpy-porosity formulation. The liquid-solid mushy zone is treated as a porous zone with porosity equal to the liquid fraction, and appropriate momentum sink terms are added to the momentum equations to account for the pressure drop caused by the presence of solid material. Sinks are also added to the turbulence equations to account for reduced porosity in the solid regions.

• Multiphase Volume of Fluid (VOF): The VOF model is a surface-tracking technique applied to a fixed Eulerian mesh. It is designed for two or more immiscible fluids where the position of the interface between the fluids is of interest. In the VOF

model, a single set of momentum equations is shared by the fluids, and the volume fraction of each of the fluids in each computational cell is tracked throughout the domain.

• UDFs: Besides the built-in standard models, FLUENT offers User Defined Functions, or UDFs, that allows the implementation of new user models and the extensive customization of existing ones. A UDF is a function written in the C programming language that can be dynamically loaded with the ANSYS FLUENT solver to enhance the standard features of the code. UDFs are either compiled or interpreted, and the macros' names are loaded in a library for ready use. Depending on macro type, these functions can be selectable from suitable zones where it can be implemented.

• Species transport: The FLUENT solidification and melting model in the version used can work along with species transport to cover mass transfer solution between phases in the domain during the phase change. In addition to basic equations in solidification/melting and VOF models, new sets of species transport equations are solved for the total mass fraction of each species in every phase, which makes the case much more complicated and computationally expensive. Heat transfer, solidification & melting models and UDFs are actually used in this work. The mass transfer calculation is modeled by UDFs instead of the species transport model.

1.4.2 FLUENT Limitations

Besides the above capabilities, FLUENT has the following limitations. Since FLUENT is a general solver, it cannot cover all aspects of physical phenomena present in engineering problems. For example, during the course of defrost on refrigeration evaporators, frost will evaporate and sublimate into the surrounding environment, even at

very low temperature. The evaporation and sublimation of frost are described in many textbooks and papers [13, 14]. The driving mechanism is the difference in the partial pressure of water vapor between the frost surface and the surrounding air. However, the evaporation models that are included in FLUENT are temperature-based.

Lastly, of the general multiphase models (VOF, mixture, and Eulerian) that FLUENT currently uses, only the VOF model can be used with the solidification and melting model.

1.5 Objectives

The objectives of this thesis are: (1) to apply a commercially available CFD software to simulate the melting of frost coupled with the heat and mass transfer processes taking place on the evaporator during defrosting, and (2) to use the model to investigate the thermal response of the evaporator and defrost time for different hot gas temperatures and frost densities.

Chapter 2. COMPUTATIONAL MODEL

2.1 Evaporator Geometry

Evaporators consist of many rows of tubes on which fins are attached. The fins increase surface area, which improves heat transfer to or from the air passing over the fins. The heat transfer of an evaporator coil is dependent on fin pitch (number of fins per inch), fin height, fin material and method of attachment. Depending on the application, the tube and fin materials can be of copper, aluminum, or stainless steel.

In this thesis, the evaporator from LRC Coil Company is introduced and analyzed. Table 1 summarizes some basic geometries of the LRC evaporator. More details of this evaporator can be found in Appendix A.

Table 1. Basic geometries of the evaporator

Specifications	Values
Evaporator Model	LRC DX1210
Fin Pitch, mm	5.48
Fin thickness, mm	0.101
Outside tube diameter, mm	16.84
Inside tube diameter, mm	15.31
Tube pitch • Tube transverse pitch, mm • Tube longitudinal pitch, mm	Staggered 44.45 38.1

2.2 Computational Domain

As shown in Figure 2, the coil is divided into similar portions, which include a tube section and rectangular section of fin attached to it. The model can be simplified by assuming vertical symmetric planes as shown in Figure 3. The boundary conditions are discussed further in Section 2.5.

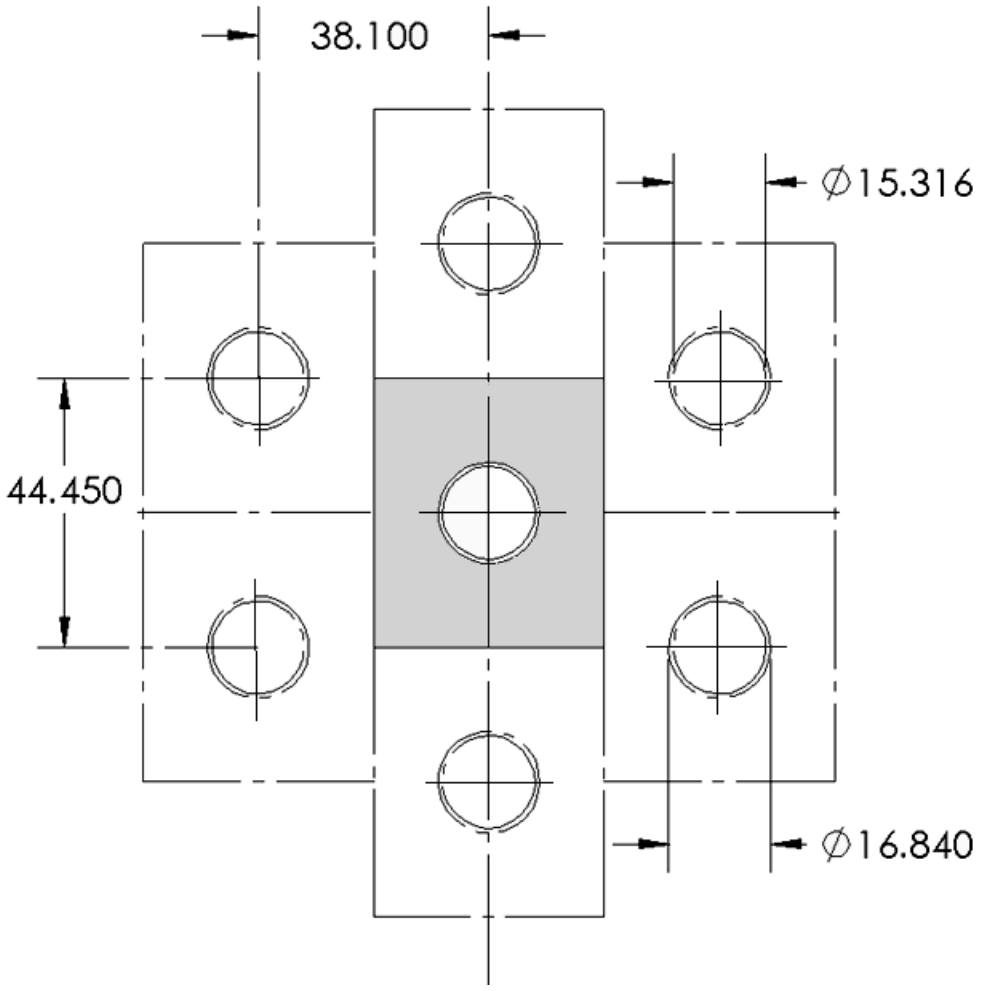

Figure 2. A section of tube and rectangular fin on the evaporator (dimensions in mm)

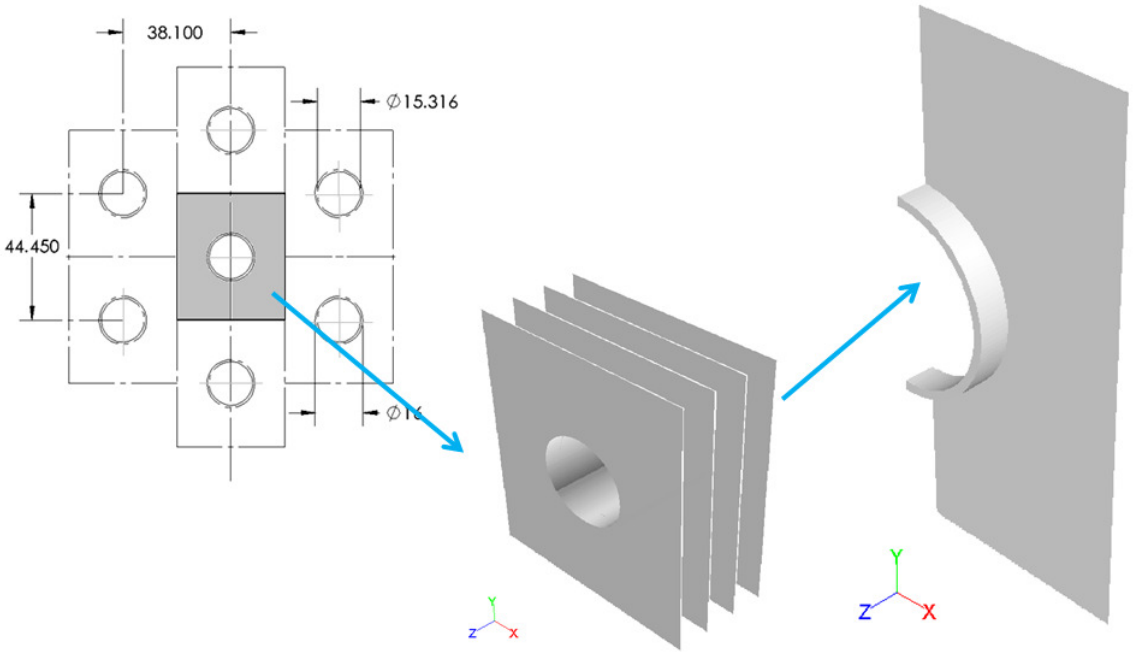

Figure 3. Final calculation domain

2.3 Mesh Generation

The geometry is created in Gambit, or using CAD software such as Solidworks, and the mesh is generated by Gambit. Different cell sizes are assigned to different regions of the domain depending on the nature of the fluid flow. In addition, the VOF model requires a fine mesh near the free surface, which is an inherent limitation of the VOF method. Therefore, the cell size in the frost layer is kept small enough so that there will not be large variations in size from the neighboring fin region and frost layer region.

Two sets of meshes have been created to test the independence of the grid on the simulation's results. They differ in mesh size and spacing interval on some edges of the domain. Figure 4 and Figure 5 show the final meshed computational domains. In these

figures, the mesh of the fin-tube domain is on the right and the whole domain, which includes the fin-tube and the air-frost domain, is on the left. Table 2 summarizes the basic settings in generating these two meshes.

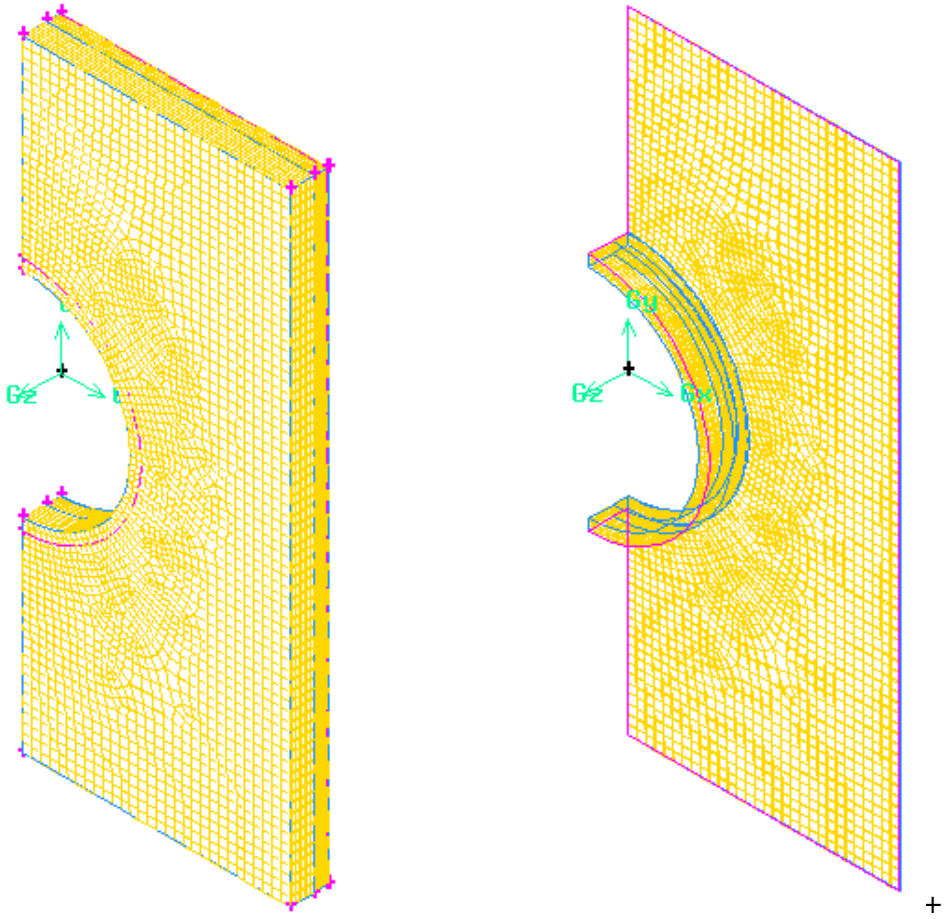

Figure 4. Mesh A (fine mesh) with 44,118 cells, average cell size ≈ 0.347mm

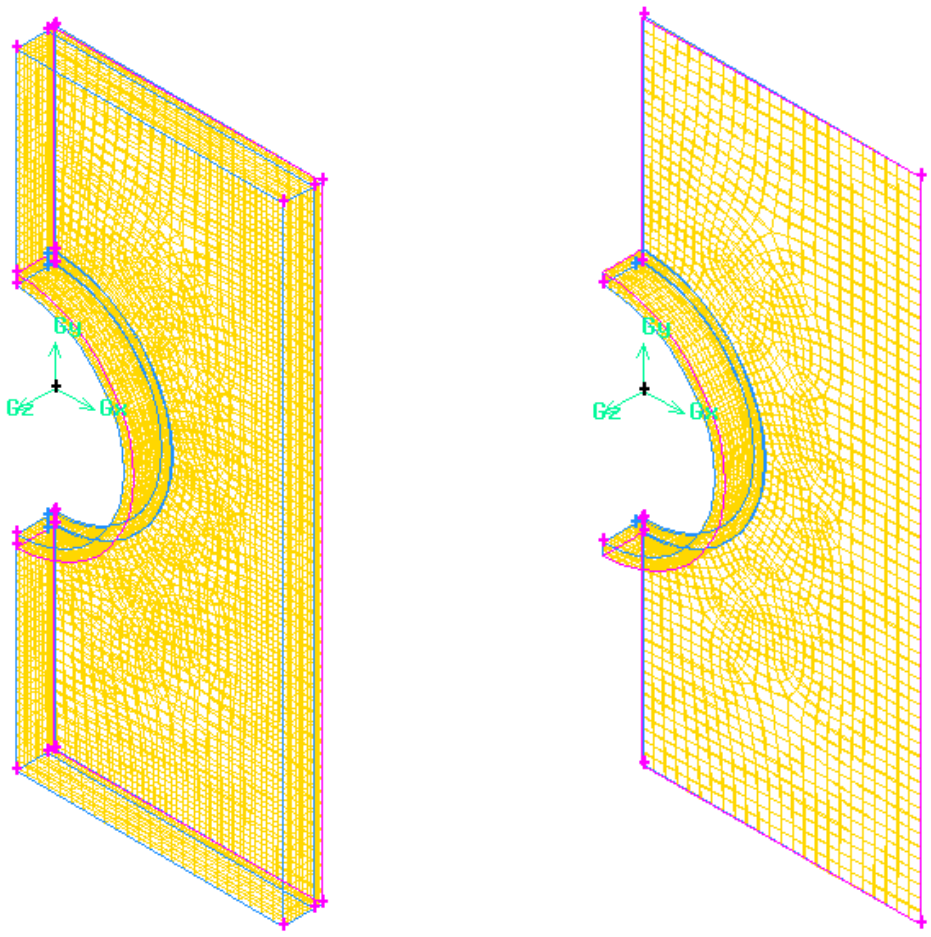

Figure 5. Mesh B (coarse mesh) with 24,724 cells, average cell size ≈ 0.423mm

Table 2. Basic settings used to generate mesh in Gambit 2.4

Variables	Mesh A	Mesh B
Mesh size	44,118	24,724
Solver	Fluent 5/6	Fluent 5/6
Mesh Face Scheme	Quad - Map	Quad - Map
Mesh Volume Scheme	Hex/Wedge - Cooper	Hex/Wedge - Cooper
Spacing- Interval size [mm]	Fin-Tube grid: 0.125-0.388 Air-Frost grid: 0.125-0.531	Fin-Tube grid: 0.125-0.481 Air-Frost grid: 0.125-0.794
Mesh dimensions	22mm x19.05mm x 2.745mm	22mm x19.05mm x 2.745mm

2.4 Mathematical Formulation

The properties appearing in the transport equations are determined by the presence of the component phases in each control volume. For example, in a two-phase system including air and frost, if the air and frost phases are represented by the subscript 1 and 2, respectively, and if the volume fraction of frost is being tracked, the average density of each cell, ρ, is given by:

$$\rho = \alpha_2\rho_2 + (1 - \alpha_2)\rho_1 \quad (1)$$

where

ρ_1= air density

ρ_2 = frost density

α_1 = volume fraction of air phase

α_2 = volume fraction of frost phase

According to (1), when frost melts and runs out of cell ($\alpha_2 = 0$), the average cell density would be the air density ($\rho = \rho_1$). In general, for an n-phase system, the volume-fraction-averaged density takes on the following form:

$$\rho = \sum_{q=1}^{n} \alpha_q \rho_q \quad (2)$$

The governing transport equations are summarized in the following sections.

2.4.1 Continuity Equation

$$\frac{\partial \rho}{\partial t} + \nabla.(\rho \overrightarrow{V}) = 0 \tag{3}$$

2.4.2 Momentum Equation

A single momentum equation is solved throughout the domain, and the resulting velocity field is shared among the phases. The momentum equation, shown below, is dependent on the volume fractions of all phases through the properties ρ and μ:

$$\frac{\partial}{\partial t}(\rho\vec{v}) + \nabla.(\rho\vec{v}\vec{v}) = \nabla.[\mu(\nabla\vec{v} + \nabla\vec{v}^{\mathrm{T}})] - \nabla P + \rho\vec{g} + \vec{S} \tag{4}$$

The momentum source/sink term, *S*, contains contributions from the porosity of the mushy zone, the surface tension along the interface between the two phases, and any other external forces per unit volume.

2.4.3 Energy Equation

The energy equation, also shared among the phases, is shown below:

$$\frac{\partial}{\partial t}(\rho H) + \nabla.\left(\vec{v}(\rho H)\right) = \nabla.\left(k_{eff}\nabla T\right) + S_h \tag{5}$$

The enthalpy H is a mass-averaged variable and calculated as following:

$$H = \frac{\sum_{q=1}^{n} \alpha_q \rho_q H_q}{\sum_{q=1}^{n} \alpha_q \rho_q} \tag{6}$$

where H_q for each phase is based on the specific heat of that phase and the shared temperature. The properties ρ and k_{eff} (effective thermal conductivity) are shared by the

phases. The source term, S_h, contains contributions from convection, latent heat transfer due to phase change and any other volumetric heat sources.

The enthalpy of the material is computed as the sum of the sensible enthalpy, h, and the latent heat content, ΔH:

$$H = h + \Delta H \tag{7}$$

where

$$h = h_{ref} + \int_{T_{ref}}^{T} c_p dT \tag{8}$$

and h_{ref} = reference enthalpy

T_{ref} = reference temperature

c_p = specific heat

The liquid fraction, λ, can be defined as

$$\begin{aligned} \lambda &= 0 && \text{if } T < T_{sol} \\ \lambda &= 1 && \text{if } T > T_{liq} \\ \lambda &= \frac{T - T_{sol}}{T_{liq} - T_{sol}} && \text{if } T_{sol} < T < T_{liq} \end{aligned} \tag{9}$$

The latent heat content is expressed as:

$$\Delta H = \lambda L_{fus} \tag{10}$$

and can vary between zero (for a solid) and L_{fus} (for a liquid).

2.5 Boundary conditions

After initializing the preliminary boundary conditions in Gambit, the geometry is exported to FLUENT for detailed boundary settings. The domain is subdivided into the air-frost and the fin-tube sub-domains with boundary conditions as shown in Figure 6. The surrounding boundaries, where air can circulate through the domain to the surrounding freezer air are pressure outlets. The left, top and bottom walls of the frost layer are assumed to be adiabatic. The bottom side of the frost layer is in direct contact to the fin and tube surfaces. There are two symmetric planes perpendicular to the tube axis. One bisects a single fin and the other is halfway between two adjacent fins. The third symmetry plane runs though the tube axis and divides the tube into two equal, semi-cylindrical shapes. Further details in the boundary conditions are given in Table 3.

A constant surface tension is specified on the "Phase Interaction" menu and a no-slip boundary condition is imposed on the walls where fluid and solid meet. The simulation is initiated assuming the fin temperature is a constant 244K, which is the temperature of the refrigerant at the end of refrigeration phase. The temperature of surrounding air in the cold room assumed to be 258K with a relative humidity of 80%. The initial temperature of frost layer is assumed to be 258K. The hot gas refrigerant is modeled as a constant temperature heat source applied on the inner side of the tube surface. Three different temperatures are used for the heat source: 283K, 293K, and 303K corresponding to different hot gas refrigerant temperatures. The simulation is run under normal atmospheric pressure.

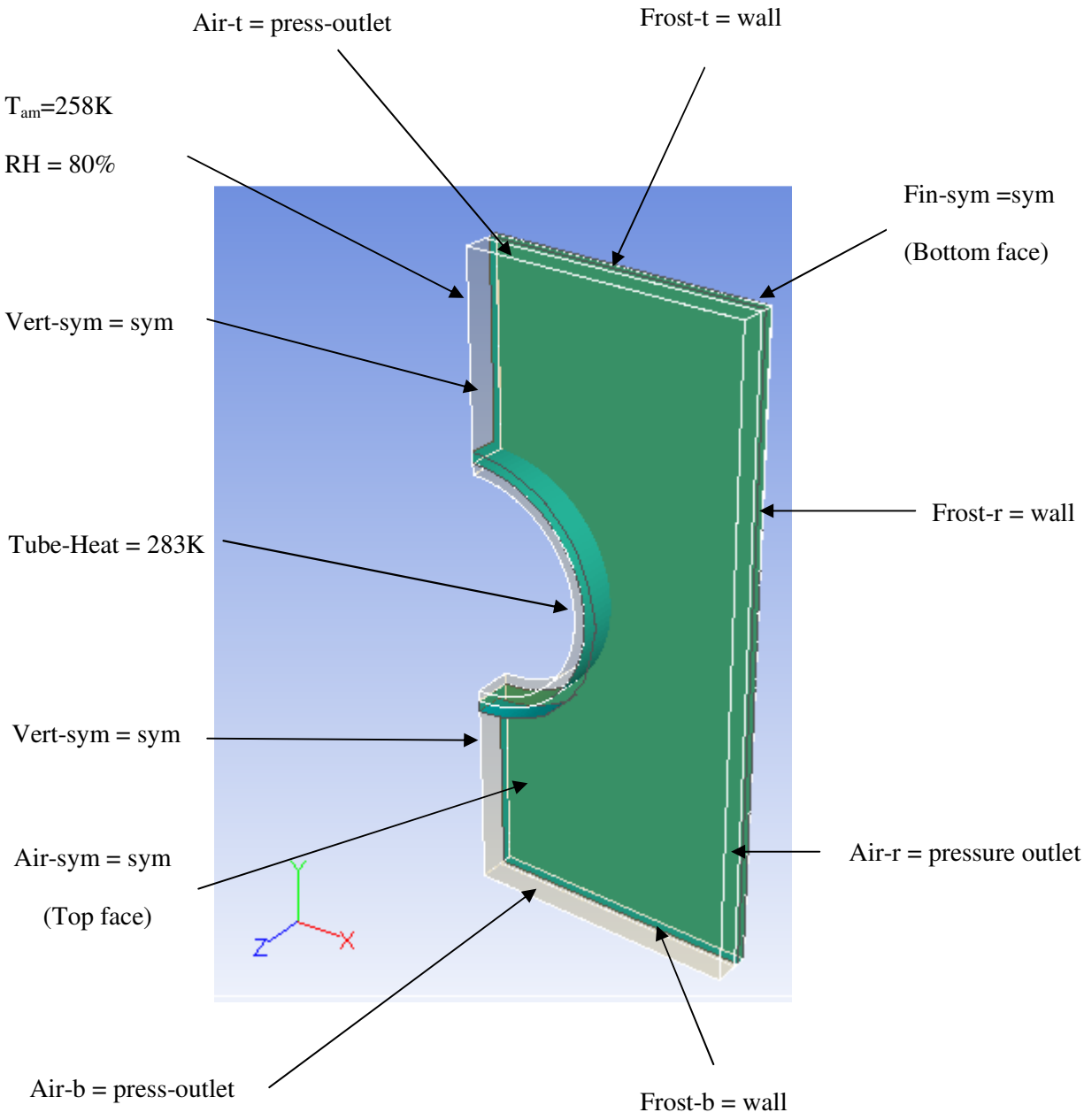

Legends: t = top, b = bottom, r = right, sym = symmetric boundary.

Figure 6. Boundary conditions

Table 3. Boundary settings

Boundary / Zone Name(s)	Settings
Air-t, Air-r, Air-b	Pressure outlet
Air-sym, Fin-sym-bot, Vert-sym	Symmetry
Frost-t, Frost-r, Frost-b	Wall
Tube-heat	Constant temperatures: 283K, 293K and 303K.
Surface Tension, [N/m]	0.0719
Mushy Zone Constant	1.6×10^6
$T_{am,}$ [K]	258
Relative Humidity, [%]	80

2.6 Material Properties

2.6.1 Frost Properties

The frost layer can be considered a mixed material of ice crystals and humid air surrounding them. Accordingly, many types of formulas have been proposed for the prediction of thermal conductivity depending upon how the mixed construction is modeled. In practical engineering, experimental formulas were proposed which yield more precise predictions, although most were not always based on physically reasonable explanations. They were mainly expressed as functions of frost density [15]. Recently, Iragorry et al. [16] conducted a series of experiments and suggested the following approximation for the effective thermal conductivity, $\overline{k_{eff}}$, of a porous matrix consisting of ice and air:

$$\overline{k_{eff}} = 0.02422 + 7.214 \times 10^{-4}\rho_f + 1.01797 \times 10^{-6}\rho_f^2 \quad (11)$$

where, ρ_f is frost density.

This relationship is shown in Figure 7. Additional properties for the frost layer are given in Table 4.

Table 4. Frost properties

Properties	Value
Temperature reference, [K]	273.15
Density, [kg/m^3]	150, 300, 450
Solidus Temperature, [K]	271
Liquidus Temperature, [K]	274
Thermal conductivity, [W/m-k]	0.15,0.325, 0.55
Specific Heat, [J/kg-K]	2040
Molecular Weight, [kg/kg-mol]	18

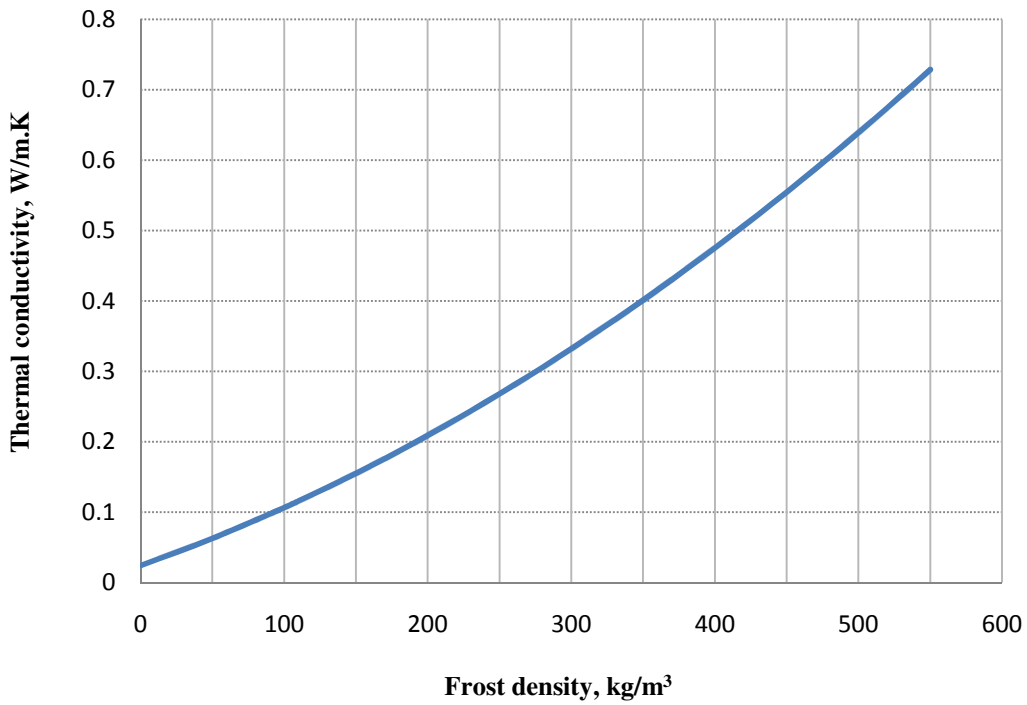

Figure 7. The effective frost conductivity according to Iragorry et al. [16]

2.6.2 Air Properties

The air properties are listed in Table 5.

Table 5. Air properties

Properties	Value
Temperature reference [K]	273.15
Density, [kg/m^3]	1.270
Thermal conductivity, [W/m-k]	0.025
Specific Heat, [J/kg-K]	1006
Viscosity, [Ns/m^2]	0.18x10^{-4}
Molecular Weight, [kg/kg-mol]	28.996
Thermal Expansion Coefficient, [1/K]	0.0035

2.6.3 Fin and Tube Properties

In this work, aluminum is used as the material for both the tube and fin. Table 6 summarizes the aluminum properties.

Table 6. Aluminum Properties

Property	Value
Density, [kg/m^3]	2719
Thermal conductivity, [W/m-k]	202
Specific Heat, [J/kg-K]	871

2.7 Heat transfer from frost to air

The air flow regime during the defrost process is dominated by natural convection, as described in many papers. To simplify the heat and mass transfer calculations for the complex geometry of a finned tube evaporator, correlations for either

horizontal tube or flat vertical plates are used. There are many correlations available in the published literatures that are applied for different geometries. In this work, the correlation for a flat vertical plate from Jaluria [17] is used. The correlation is:

$$Nu_L = 0.13(Ra)^{1/3} \qquad \text{for } 10^9 < Ra < 10^{13} \tag{12}$$

where *Ra* is the Rayleigh number, a product of the Grashof and Prandtl numbers:

$$Ra = GrPr \tag{13}$$

$$Gr = \frac{\left(\frac{\Delta \rho}{\rho_M}\right)}{\nu^2} . g . L^3 \tag{14}$$

$$\Pr = \frac{\nu}{\alpha} \tag{15}$$

In the Grashof equation, $\Delta\rho$ is density difference between saturated air at the surface and the surrounding air, and ρ_M is the average density of the air mixture in the domain.

The Nusselt number is used to estimate the convective heat transfer coefficient according to the following equation:

$$\overline{h_f} = \frac{k_a}{L} Nu_L \tag{16}$$

2.8 Mass transfer from frost to air

Unlike the evaporation of water driven by increasing temperature to the boiling point, during defrost the evaporation of water to the air is driven by the difference in partial pressures of the water vapor at the frost surface and the air.

Aljuwayhel [18] suggested that frost sublimation along with water evaporation can occur during defrost. The mechanism for frost sublimation is based on the same principle as water evaporation, and the mass transfer coefficient is assumed to be equal for both evaporation and sublimation [18]. The latent heat due to evaporation, q_{evap}, and sublimation, q_{sub}, are calculated based on the following equations:

$$q_{evap} = h_m A L_{evap}(\rho_{w.sat} - \rho_{w.am}) \quad (17)$$

$$q_{sub} = h_m A L_{sub}(\rho_{w.sat} - \rho_{w.am}) \quad (18)$$

where A= Air-frost interface area

h_m= mass transfer coefficient

L_{evap}= Latent heat of evaporation

L_{sub}= Latent heat of sublimation

$\rho_{w.sat}$= Density of water vapor at frost surface

$\rho_{w.sat}$= Density of water vapor at freezer ambient temperature

The mass transfer coefficient is calculated by using the analogy between convective heat transfer and convective mass transfer and the Nusselt number, *Nu*, is replaced by the Sherwood number, *Sh*, and the Prandtl number, *Pr*, is replaced by the Schmidt number, *Sc* [17].

$$Sh_L = 0.13(GrSc)^{1/3} \qquad \text{for } 10^9 < \text{GrSc} < 10^{13} \quad (19)$$

The Schmidt number is defined as:

$$Sc = \frac{\nu_a}{D_{w2a}} \quad (20)$$

where v is kinematic viscosity of the air, and D_{w2a} is the mass diffusivity of the water vapor in the air. The function for the diffusion coefficient of the water in air is obtained using the regression curve fit to the data Bolz and Tuve (1976):

$$D_{w2a} = -2.775x10^{-6} + 4.479x10^{-8}T + 1.656x10^{-10}T^2 \quad (21)$$

The convective mass transfer coefficient is then calculated as:

$$h_m = \frac{\rho_M Sh_L D_{w2a}}{L} = \frac{\rho_M Sh_L \nu}{LSc} \quad (22)$$

A User Defined Function (UDF) was written because FLUENT does not provide an algorithm for calculating frost evaporation and sublimation. The UDF is written in C and incorporated into FLUENT through a compiler or interpreter. The theory and equations for mass transfer mechanism are presented above, while the UDF code is listed in Appendix B.

2.9 Assumptions

In the development of the model, the following assumptions are made:

- The melt is assumed to be a Newtonian fluid and incompressible.
- Fluid motions in the melt are assumed to be laminar.
- The Boussinesq approximation for natural convection flow is applicable since the variation in density with respect to the reference density is small.
- The effects of volume change associated with the solid to liquid phase change are negligible.
- The refrigerant temperature is constant.

- The specific heat and thermal conductivity of the frost material are considered constants.
- The properties (density, specific heat and thermal conductivity) of the frost and water are the same.
- Pure substances like water solidify without a mushy zone. According to Voller [19], for phase changes of pure water, the temperature difference between T_{liq} and T_{sol} is introduced for numerical convenience, typically up to 0.5K. In reality, during the formation and accumulation of frost on commercial and industrial evaporators, ice is mixed with air, airborne particles and other substances in the freezer environment. Therefore, frost is not considered a pure material and the value of T_{sol} can be set as low as 271K, while the value of T_{liq} is around from 273K to 274K [20,21]. In this work, T_{sol} is set at 271K and T_{liq} is set at 274K.

Appendix C provides the CFD modeling overview of hot gas defrost problem.

Chapter 3. SIMULATION SETUPS AND RESULTS

3.1 Simulation setups:

In the Models panel (accessed by Define > Models), the solidification and melting model is activated with the mushy zone constant set to $1.6x10^6$ and the multiphase model turned on with the VOF option. The simulation is conducted with very small initial time step sizes. A summary of the model settings are given in Table 7.

The calculations employ the PISO (Pressure Implicit with Splitting of Operators) algorithm for pressure-velocity coupling and the first order upwind scheme for the determination of momentum and energy. Although the higher order scheme can result in greater accuracy, it can also result in convergence difficulties and instabilities. For most preliminary solutions, the first order scheme yields an acceptable accuracy. At the beginning of the simulation, the time step size is set to 10μs and then increased to between 1ms and 5ms towards the end of simulations, depending on the percentage of frost and air in the domain. The time step adjustment is made manually by direct observation of the residuals during the simulation. Within several consecutive calculation steps, if the simulation reaches the maximum number of iterations per step and cannot converge, a smaller time step size is applied.

For spatial discretization, the QUICK scheme (Quadratic Upstream Interpolation Convective Kinematics) is chosen because the case employs hexahedral meshes. The QUICK scheme is based on a weighted average of second order upwind and central interpolations of the variable. Other solution method settings are given in Table 8.

Table 7. Basic settings of CFD simulation

Parameters / Models	Settings
Spatial and time settings	3-D simulation Gravity activated
Solver	Pressure based solver Absolute velocity formation Unsteady state analysis (first-order implicit)
Solidification/Melting	Activated • Mushy zone constant: $1.6x10^6$ • T_{sol} = 271K • T_{liq} = 274K
Energy equation	Activated
Viscous model	Laminar
Multiphase model • Volume of Fluid	Activated with two phases • Phase Ice: Frost (Fluid) • Phase Air: Air Implicit scheme Implicit Body Forces activated
User Defined Functions	Compiled and loaded before simulation. • Function Hooks • User Defined Memory
VOF parameters	QUICK
Time step sizes	Varies from 10μs in the first 20000 steps to 1ms towards the end of simulation.

Table 8. Solution Method Settings

Solution Methods	Settings
Pressure-velocity coupling	Pressure-Implicit with Splitting of Operators (PISO)
Gradient	Green-Gauss Node based
Pressure	PRESTO!
Momentum	First Order Upwind
Volume Fraction	QUICK
Energy	First Order Upwind
Transient Formulation	First Order Implicit

There are eleven simulation cases which are set up and run with different input temperatures, frost densities, and mesh sizes. Besides these differences, all boundary and initial conditions, and other settings are kept the same for all cases. The cases are numbered and listed in Table 9. Among these cases, Case 4 and Case 7, which use Mesh A (see Figure 4), are used as baseline cases to compare with Case 10 and Case 11, which use Mesh B (see Figure 5), respectively. The simulation results from these pairs of cases are compared to test the grid independence of the model. Details of the comparisons are given in Section 3.3.1.

Due to the lack of computer resources, all of the simulations are run with 0.5 mm of frost, and for the grid independency test, only coarser meshes are considered.

Table 9. Case Settings and Numeration

Case	Basic Settings	Mesh Type
1	ρ =150 kg/m^3, T_{hot}=283 K	A
2	ρ =150 kg/m^3, T_{hot} =293 K	A
3	ρ =150 kg/m^3, T_{hot} =303 K	A
4	ρ =300 kg/m^3, T_{hot} =283 K	A
5	ρ =300 kg/m^3, T_{hot} =293 K	A
6	ρ =300 kg/m^3, T_{hot} =303 K	A
7	ρ =450 kg/m^3, T_{hot} =303 K	A
8	ρ =450 kg/m^3, T_{hot} =303 K	A
9	ρ =450 kg/m^3, T_{hot} =303 K	A
10	ρ =300 kg/m^3, T_{hot} =283 K	B
11	ρ =450 kg/m^3, T_{hot} =283 K	B

3.2. Solution convergence and solution monitoring

The discretized forms of the governing equations are solved numerically for the velocity and pressure values across the domain by using iterative methods. Iterative methods are approximate methods, which start with an initial guess and iterate to a converged solution with some pre-specified tolerance limits. FLUENT uses Gauss-Seidel iteration with a multigrid scheme to accelerate the convergence of the solver.

A solution is said to be converged when the difference between the process values obtained at two consecutive iterations is less than a residual amount which can be set by the user. The residual is defined as the imbalance of the linear discretized equations and

are useful indicators of solution convergence. For most problems, the default residuals specified by ANSYS FLUENT (Table 10) are sufficient [11]. The convergence is checked by direct observation of the residuals during the simulation. In all cases, the calculated residuals must be less than the preset values (see Figure 8).

The FLUENT pressure-based solver uses under-relaxation of equations to control the update of computed variables at each iteration and stabilize the convergence behavior of the outer nonlinear iterations. The optimal under relaxation factors specified by FLUENT are used in most cases and can be reduced if the convergence difficulty occurs. The values of the under relaxation factors are listed in Table 11.

Table 10. Residual Settings

Residuals	Values
Continuity	10^{-3}
Velocity components (x, y, z)	10^{-3}
Energy	10^{-5}

Table 11. Under-Relaxation Factors

Under-Relaxation Factors	Values
Pressure	0.2
Density	0.5 to 1
Body Forces	0.5 to 1
Momentum	0.2
Volume Fraction	0.7 to 1
Liquid Fraction Update	0.5 to 1
Energy	0.98 to 1

During the simulation, the volume integral of the frost phase was monitored to check for melting. The simulation was stopped when the amount of frost in the domain was less than 1% of its initial volume (see Figure 8).

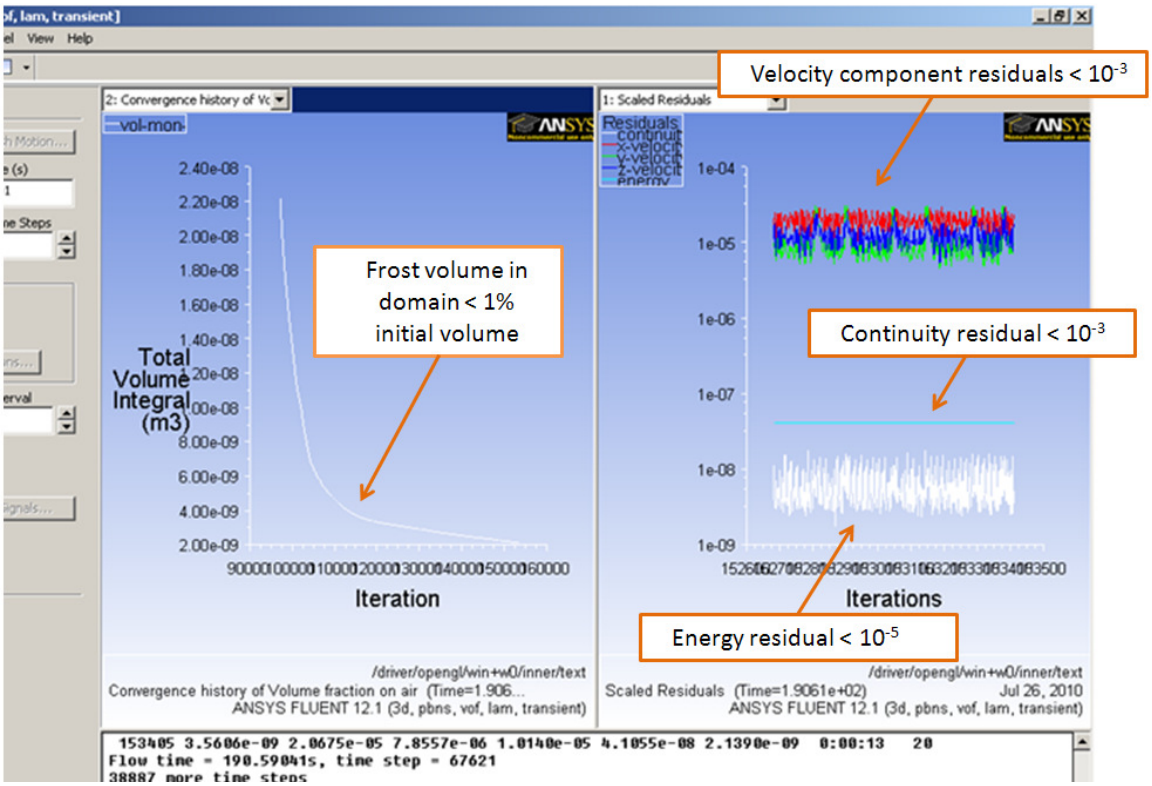

Figure 8. Monitoring the frost volume and residuals

3.3 Simulation results and discussion

The model is developed with the geometry of the LCR coil and a set of boundary conditions common to industrial refrigeration [6]. A comparison of the simulation results with actual experimental data is not available to verify the accuracy of the model. This thesis highlights the effects of various parameters on the defrost process.

3.3.1 Grid independence test

Simulations are repeated with different mesh sizes to monitor the grid independence of the model. Meshes are generated by Gambit with different space intervals on edges of the fin-tube and air-frost domains. The first comparison is made between the Case 4 which uses the fine mesh (Mesh A), and Case 10 which uses a coarser mesh. Comparison criteria include melting times, volume integrals of frost left in the domain, energy input and the average air velocity. The second comparison is between Case 7 and Case 11. Table 12 and 13 detail the results from these comparisons. The percent difference is far below 15% for all results except the input energy for the second case, which is 15.03%.

Table 12. Comparison of simulation results for Case 4 and Case 10

Criteria	Case 4	Case 10	% change
Mesh Size, [cell]	44200	24724	-55.94
Frost density, [kg/m^3]	300	300	-
Initial Frost Volume, [m^3]	3.98E-07	3.98E-07	-
Time, [s]	222	209.45	-5.65
Q-in, [J]	118.33	118.98	0.55
Ave. air velocity, [m/s^2]	0.0307	0.0311	1.31

Table 13. Comparison of simulation results for Case 7 and Case 11

Criteria	Case 7	Case 11	% change
Mesh Size, [cell]	44200	24724	-55.94
Frost density, [kg/m^3]	450	450	-
Initial Frost Volume, [m^3]	3.98E-07	3.98E-07	-
Time, [s]	382.86	373.00	-2.58
Q-in, [J]	206.269	237.276	15.03
Ave. air velocity, [m/s^2]	0.0212	0.0227	6.42

Other efforts to run the cases with the finer mesh which has 74,460 cells were dropped because the simulations were extremely computational expensive with the given computer resources. The results from the above comparisons confirm that Mesh A is adequate for the model.

3.3.2 Melting time

Melting time is one of the criteria used to evaluate defrost process. The time it takes to completely melt frost from the evaporator depends on many factors, including the hot gas temperature, the temperature and relative humidity of the surrounding environment, the properties of the frost and the geometry of the evaporator. Table 14 and Figure 9 show the defrost time as a function of the frost density and the temperature of the hot gas. The melting times are directly proportional with the frost density, and inversely proportional to the input hot gas temperature. Over certain temperature range, there is not much different in melting times for different frost densities. Figure 8 shows

that the melting time does not change considerably when the hot gas temperatures is 303K and above. This observation is agreement with Hoffenbecker's results (see Figure 10) when the author analyzed the defrost times on an Imeco evaporator [6, 7].

Table 14. Melting times at different frost densities and hot gas temperatures

Frost Density [kg/m^3]	**Melting Time [s]**		
	283K	293K	303K
ρ_{frost} =150	113	48	32
ρ_{frost} =300	209	93	43
ρ_{frost} =450	373	132	57

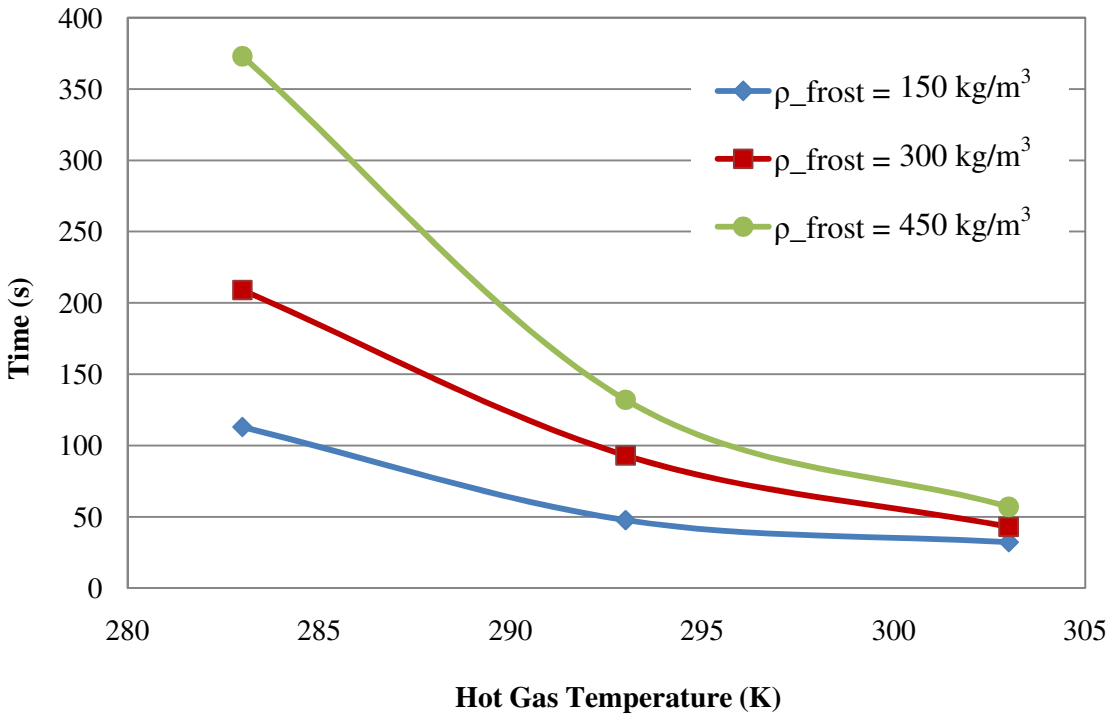

Figure 9. Melting time at various frost densities and hot gas temperatures

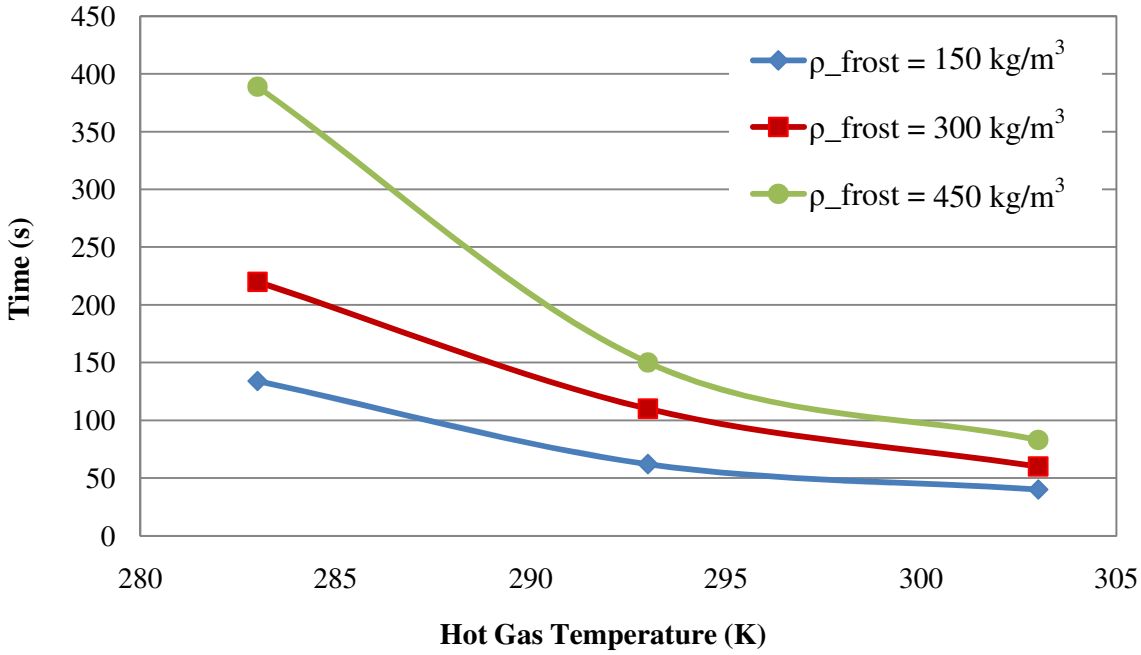

Figure 10. Melting times from Hoffenbecker's model [6, 7]

Figures 11 and 12 show the presence of the frost (blue) over time. When the frost melts, air fills the void and heat energy is then transferred directly to the surrounding air.

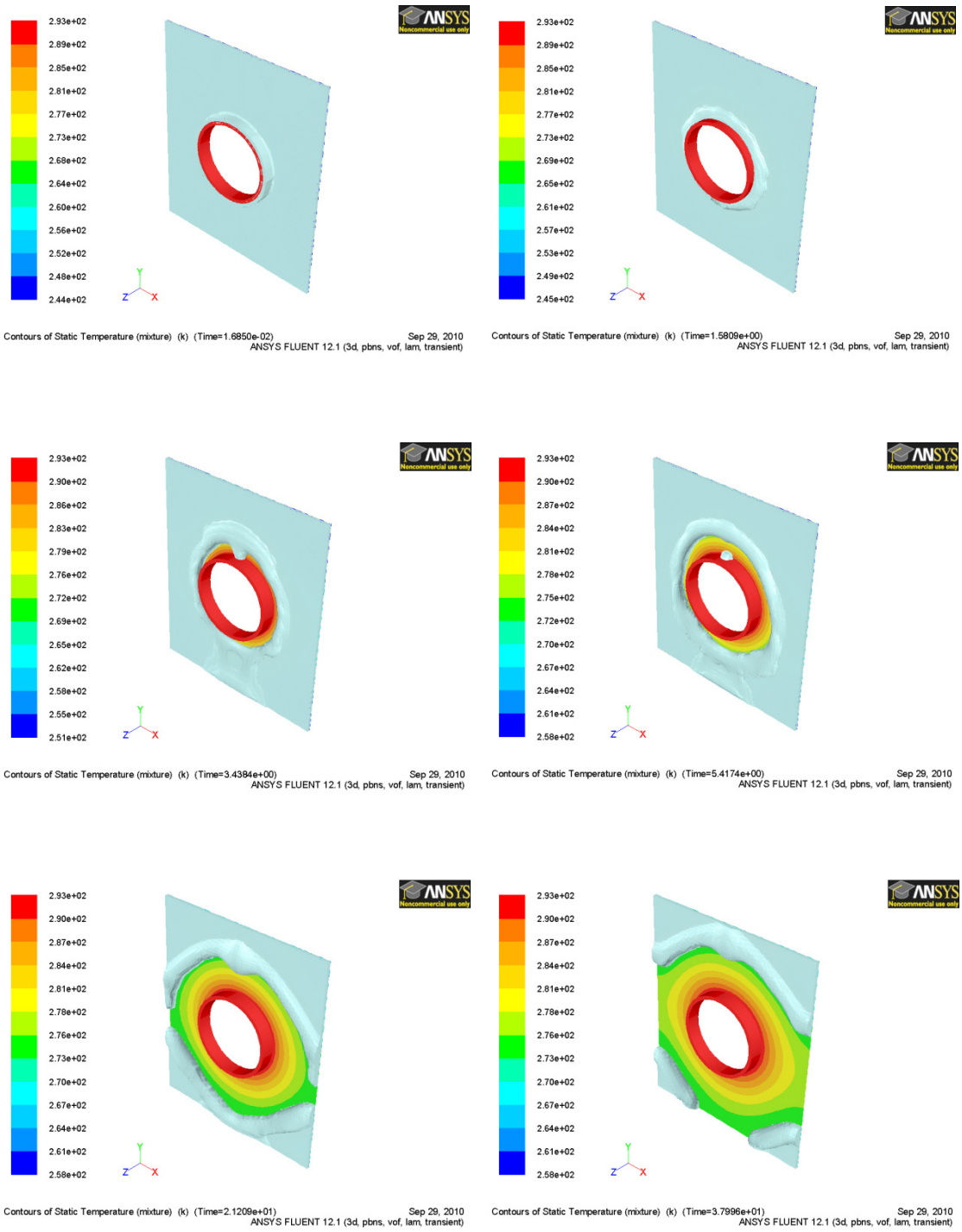

Figure 11. Interface between air and frost during defrost

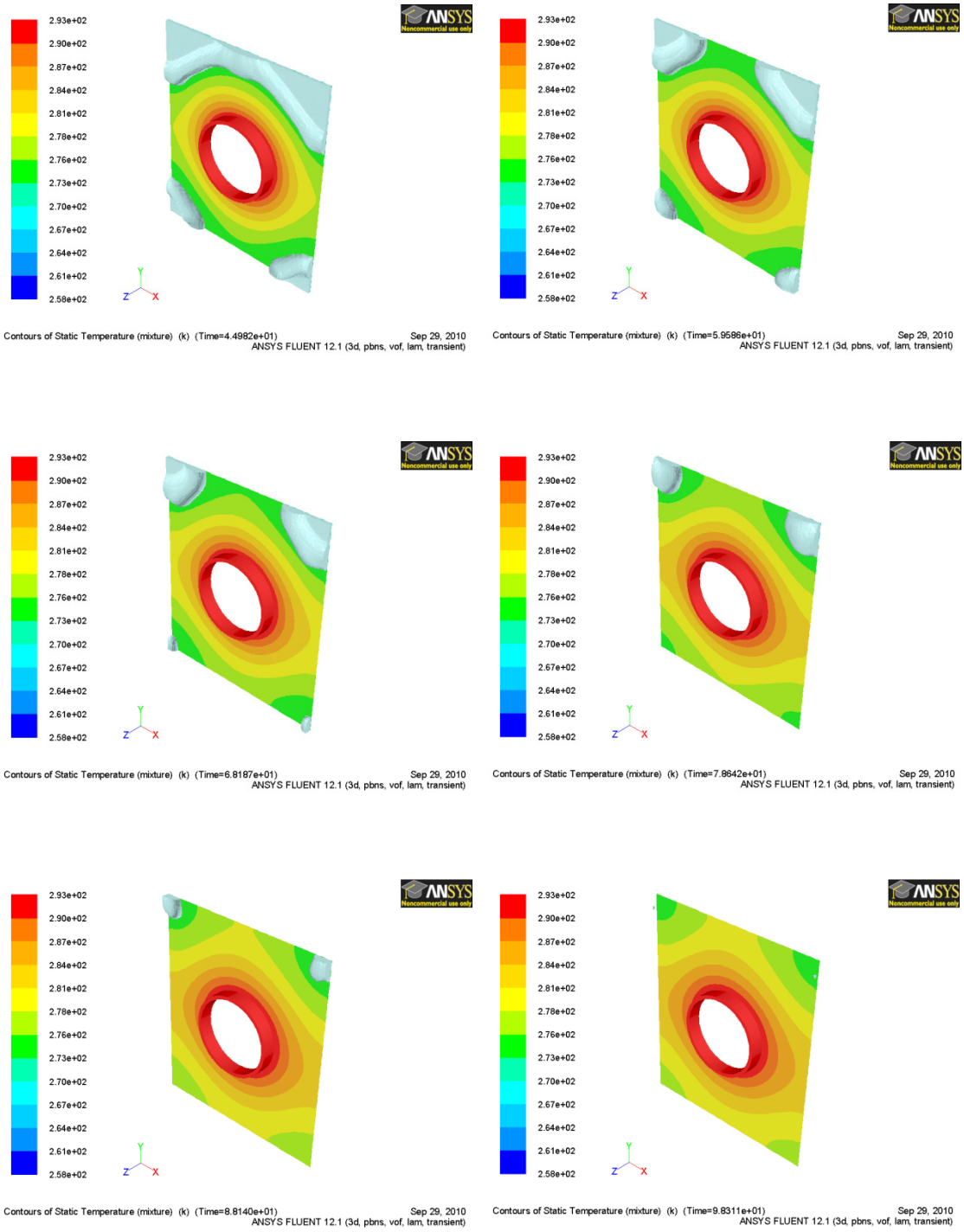

Figure 12. Interface between air and frost during defrost (cont'd)

3.3.3 Defrost Energy:

Figure 13 shows the relationship between the total energy transferred from the hot refrigerant to the domain and the hot gas temperature. The heat energy, Q_{in}, is calculated by using following equation:

$$Q_{in} = \int_0^{final\ time} \int_{A_{tube-heat}} q_{tube-heat} \,.\, dA.\, dt \tag{23}$$

where $q_{tube\text{-}heat}$ is heat flux applied on the inner wall of the tube.

It is observed that the heat input deceases as the hot gas temperature increases. Faster defrost times mean less energy is lost to the surroundings. As seen from Table 15, with ρ_{frost}= 300kg/m^3, the evaporator uses 22.7% less energy if the defrost takes place at T_{hot}=293K in comparison to defrosting at T_{hot}=283K. Above 293K, the required energy to defrost the coil decreases slightly. From these results, it is clear that defrosting at higher hot gas temperatures will reduce melting time and the input energy. Over certain temperatures, the input energy changes very slightly for ρ_{frost}= 300kg/m^3 and does not change for ρ_{frost}=150kg/m^3 and ρ_{frost}=450kg/m^3. This may suggest an "optimal temperature" setting where users can run the defrosting process with minimum input energy.

Table 15. Input Energy [MJ]

Frost density [kg/m^3]	283K	293K	303K
ρ_{frost}= 150	9.81	7.20	7.06
ρ_{frost}= 300	19.99	15.45	14.32
ρ_{frost}= 450	34.65	22.68	21.50

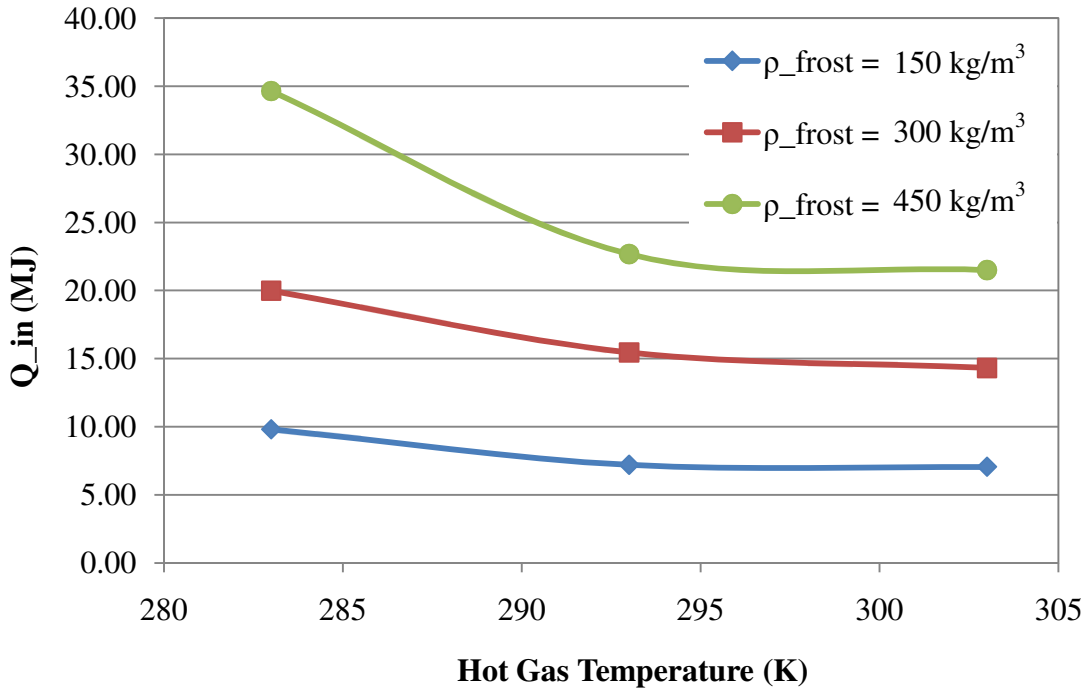

Figure 13. Input defrost energy

However, defrosting at higher temperature increases the energy stored in the fin and tube mass, which becomes a heat load after defrosting is complete. Table 16 and Figure 14 show the percentage of energy stored in the fin-tube mass ($Q_{fin,tube}$) over the total input energy at various frost densities and hot gas temperatures. At constant frost density, the percentage of energy stored in fin-tube mass increases with increasing of hot gas temperature. This is because the total heat energy decreases while the stored energy in fin-tube mass is almost the same for all cases. At a constant hot gas temperature, the lower the frost density, less energy is required to melt the frost and therefore the percentage of the energy stored in fin-tube mass increases.

Table 16. Stored energy in fin-tube mass and its percentage over input energy

Frost Density [kg/m^3]	283K		293K		303K	
	Energy [MJ]	%	Energy [MJ]	%	Energy [MJ]	%
ρ_{frost} =150	1.31	13.34	1.59	22.08	1.93	27.35
ρ_{frost} = 300	1.30	6.48	1.59	10.26	1.89	13.87
ρ_{frost} = 450	1.30	3.75	1.60	7.03	1.95	10.58

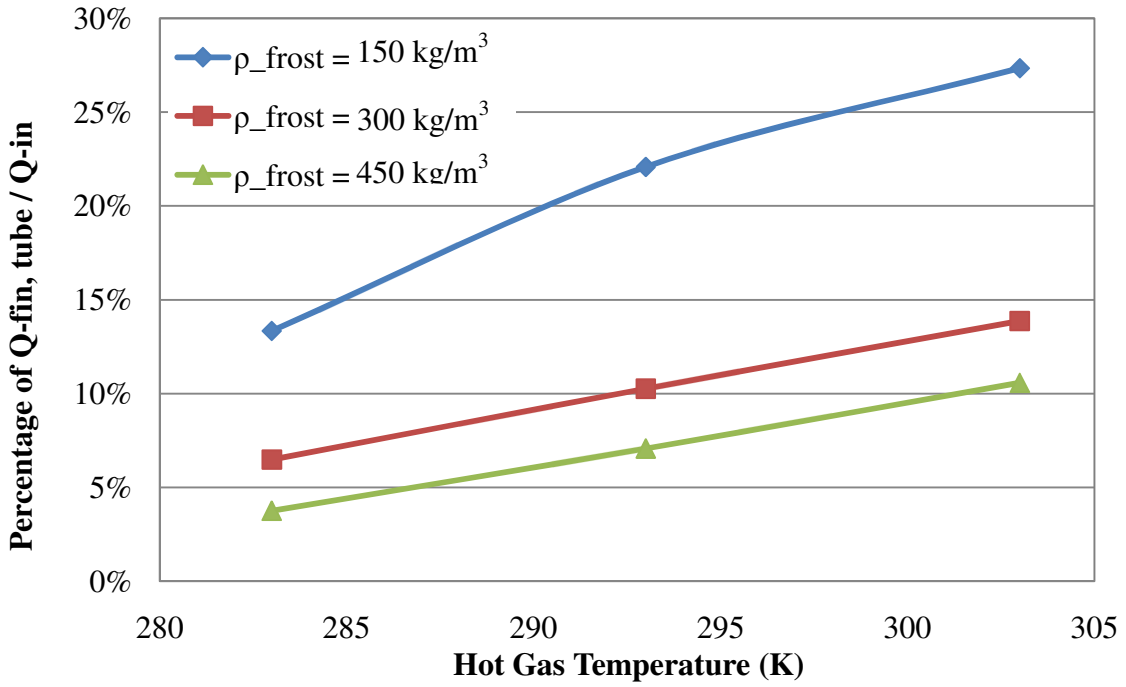

Figure 14. Percentages of stored energy in fin-tube mass vs. hot gas temperatures

3.3.4 Temperature distribution on fin surface during defrost

Figure 15 shows points on the fin surface, and Figures 16 and 17 display the temperatures of some of these points for Case 1 and Case 4. Points “ne” and “se” exhibit the lowest temperatures because their locations are furthest from the heat source.

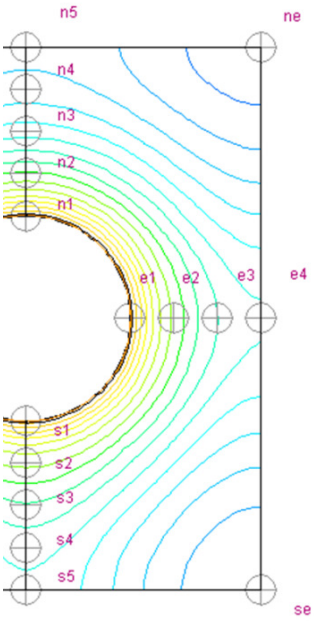

Figure 15. Points of interest on fin surface to investigate temperature distribution

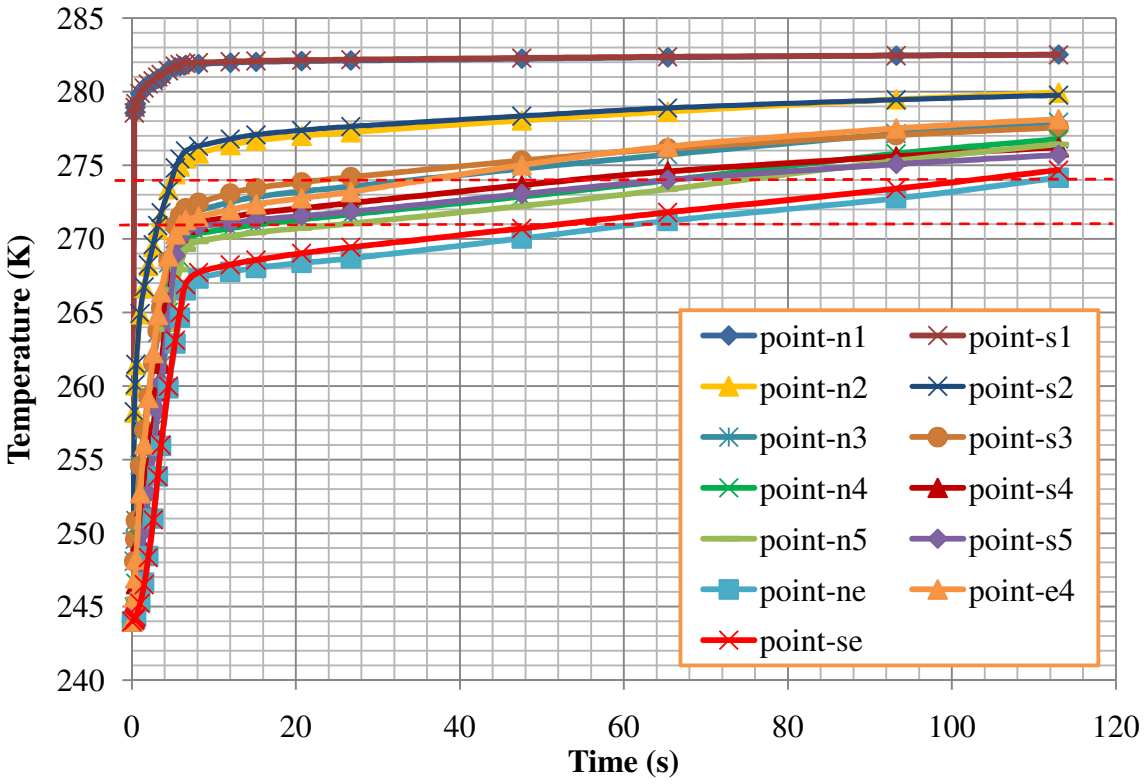

Figure 16. Fin surface temperatures at the interested points, Case 1

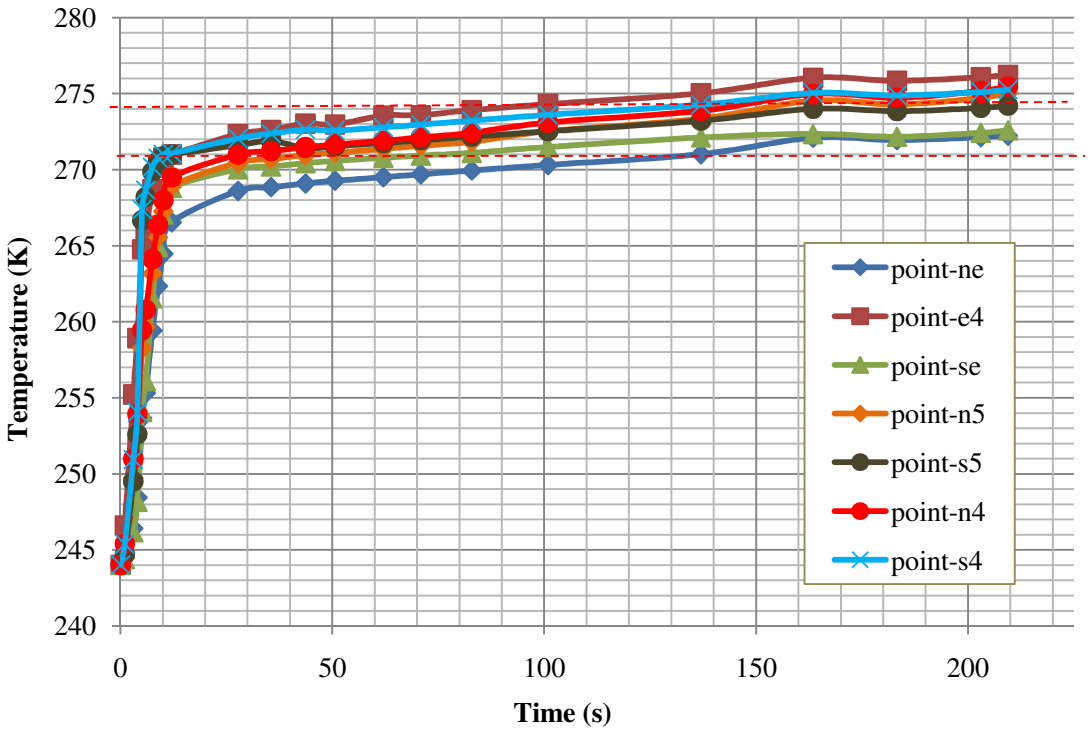

Figure 17. Fin surface temperatures at the interested points, Case 4

The fin surface temperature distribution is presented graphically in Figure 18 for Case 1. When frost is present on the fin and tube surfaces, the temperature distribution is symmetric with respect to horizontal and vertical planes cut through the domain. When the frost melts, the bottom half of the plate heats up faster due to the runoff.

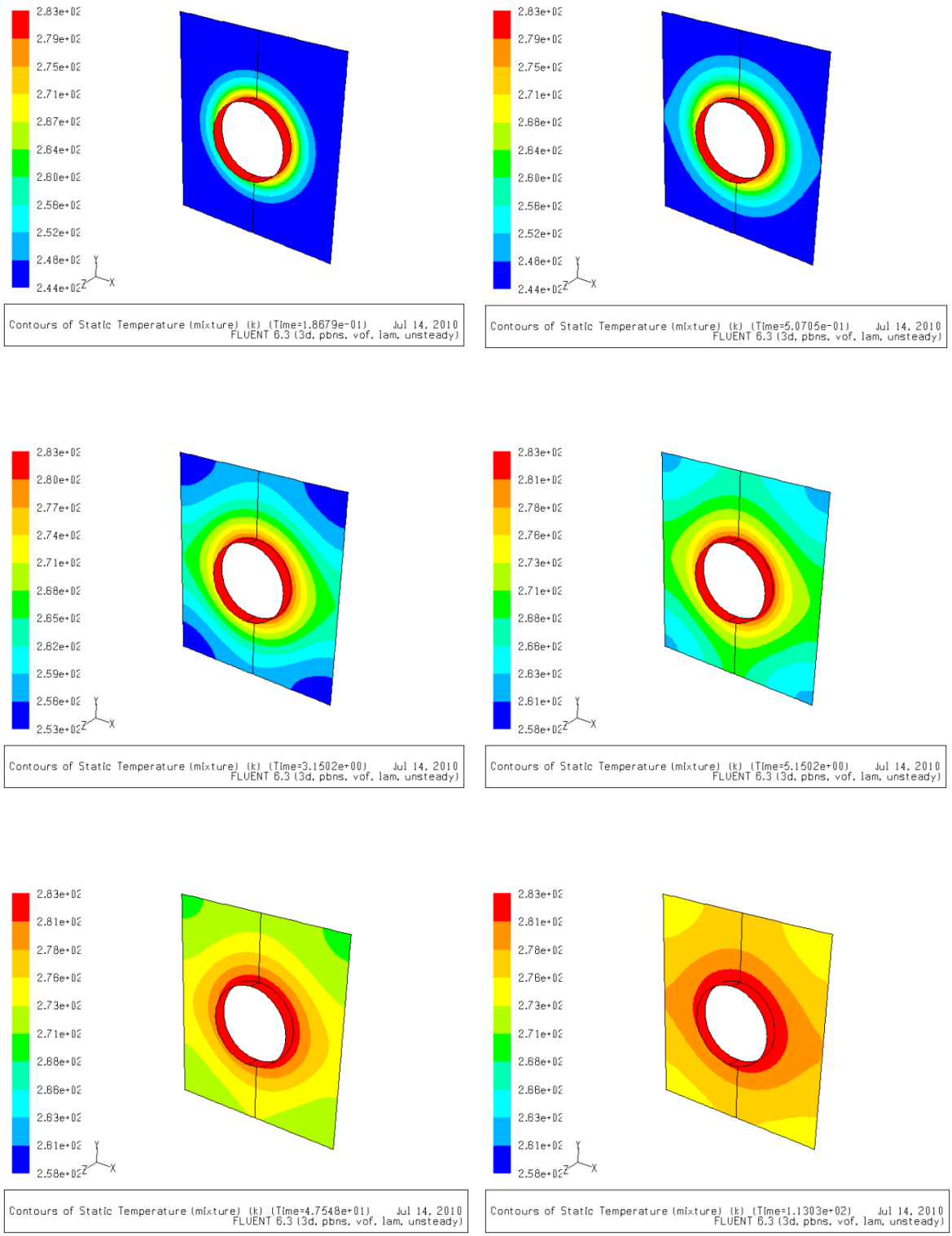

Figure 18. Fin temperature distribution during defrost, ρ=150kg/m^3, T_{hot}=283K.

Figure 19 displays the change of frost volume in the domain and the fin temperature distribution during the defrost for Case 1 (ρ_{frost}=150 kg/m^3, T_{hot}=283K) at different frost densities. The chart includes two vertical scales to represent the fin temperature (left scale) and frost volume in the domain (right scale). The defrost process is divided into three steps as seen in the figure. In the first stage, stage A, heat energy warms the tube mass, the inner part of the fin and melts the frost on the tube surface (see Figures 11, 12, and 19) at very quick rate. During the second stage, stage B, frost melts on the fin surface and leaves the domain at a slower and almost constant rate until the frost volume decreases to about 5% of the initial frost volume. In stage C, the remaining frost volume, which is in form of a water film, is removed from the domain at very slow rate.

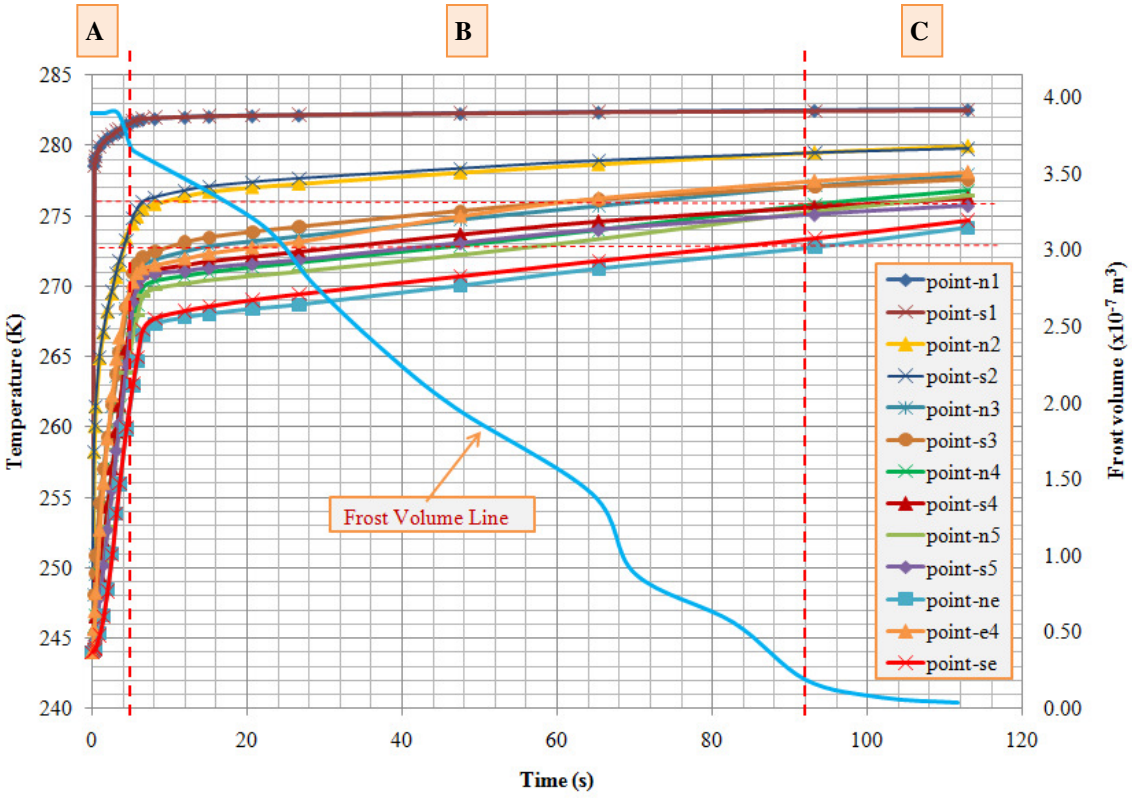

Figure 19. Fin surface temperature and frost volume vs. time, Case 4

Chapter 4. CONCLUSIONS AND RECOMMENDATIONS

4.1 Conclusions:

The melting of frost with different hot gas temperatures and frost thickness was simulated by using a commercial CFD solver, FLUENT 12.1. The simulation employed the solidification and melting model, and the Volume of Fluid (VOF) model for the frost melt interface. A User Defined Function in C language was written to model the frost evaporation and sublimation. The grid independence of the model was tested, and a comparison of simulation results between cases demonstrated that the mesh was adequate for the simulation.

The defrost time and input energy depend on many factors which include hot gas temperature, the temperature and relative humidity of the surrounding environment, the properties of the frost and the geometry of the evaporator. The simulation results show that the defrost time is directly proportional to the frost density, and inversely proportional to the hot gas temperature. Also, the input heat energy is directly proportional to the frost density and inversely proportional to the hot gas temperature. There are a trade-offs for defrosting at higher temperatures. It is shown that defrosting at higher hot gas temperatures will reduce the melting time and the input energy. However, defrosting at higher temperature also increases the energy stored in the fin and tube mass which becomes a heat load after defrosting is complete. This implies that an optimal hot gas temperature can be identified so that the defrosting process takes place with the lowest possible energy required.

4.2 Recommendation for future works

3D simulation of melting with FLUENT solver is a very computationally expensive process, especially when the program uses the VOF model, or any multiphase model. This work was completed by using a Hewlett-Packard workstation model xw4600 powered by an Intel Core 2, Dual CPU E6550 @ 2.33GHz, and physical memory of 3GB. It takes this computer around 74 hours to complete a simulation. In order to have good results, it is believed that more advanced computer resources should be used. By using computers equipped with dual core or multi-core processors, users can take advantage of the parallel computation feature and reduce the simulation time.

This work can be used as a preliminary step in using CFD to model the energy and fluid flow during defrost. The VOF model used in this project improves the calculation of heat transfer within the frost layer. However, the model itself has limitations. Frost is considered to be a homogeneous material, which shares the same thermal and physical properties with melted frost (e.g. water). There are several factors, wall adhesion, contact angle of the water and the air, and variable material properties, which should be taken into account when modeling defrosting on the finned tube evaporator. Further work needs to be done to validate the results of this study with experiments.

References

[1] Rainwater Julius H., 2009, “Five Defrost Methods for Commercial Refrigeration,” ASHRAE Journal, bookstore.ashrae.biz/journal/download.php?file=rainwater0309.pdf

[2] Parker Hannifin Corporation, 2007, “Hot Gas Defrost for Ammonia Evaporators,” Bulletin 90-11a, http://www.parker.com/literature/Refrigerating%20 Specialties% 20Division/90-11a.pdf.

[3] Krakow K.I., Yan L., and Lin S., 1992, “A Model of Hot Gas Defrosting of Evaporators - Part 1: Heat and Mass Transfer Theory,” ASHRAE Transactions 98.

[4] Krakow K.I., Yan L., and Lin S., 1992, “A Model of Hot Gas Defrosting of Evaporators-Part 2: Experimental Analysis,” ASHRAE Transactions 98.

[5] Al-Mutawa, N.K. and Sherif, S.A., 1998, "An Analytical Model for Hot-Gas Defrosting of a Cylindrical Coil Cooler: Part II-Model Results and Conclusions," ASHRAE Transactions, 104, Part 1B, pp. 1731-1737.

[6] Hoffenbecker, N., 2004, "Investigation of Alternative Defrost Strategies," Master Thesis, University of Wisconsin-Madison.

[7] Hoffenbecker, N., Klein S.A., and Reindl D.T., 2005,"Hot gas Defrost Model Development and Validation," International Journal of Refrigeration, 28, pp. 605-615.

[8] Dopazo J.A., Seara J. F, Uhia F. J., and Diz R., 2010, “Modeling and Experimental Validation of the Hot-Gas Defrost Process of an Air-Cooled Evaporator,” International Journal of Refrigeration.

[9] Dansilasirithavorn J., 2009, “Cost Minimization for Hot Gas Defrost System,” Master Thesis, California Polytechnic State University, San Luis Obispo.

[10] ANSYS, 2009, FLUENT 12.0 Theory Guide.

[11] ANSYS, 2009, FLUENT 12.0 User’s Guide.

[12] ANSYS, 2009, FLUENT 12.0 UDF Manual.

[13] Rolle, Kurt C., 1999, Heat and Mass Transfer, Pearson Education.

[14] Cheng K.C., and Seki N., 1991, Freezing and Melting Heat Transfer in Engineering, Taylor & Francis.

[15] Banaszek J., Jaluria Y., Kowalewski T.A., and Rebow M., 1999, “Semi-Implicit FEM Analysis of Natural Convection in Freezing Water,” Numerical Heat Transfer, Part A, 36, pp. 449-472.

[16] Iragorry J., Tao Y.X., and Jia S., 2004, "A Critical Review of Properties and Models for Frost Formation Analysis," HVAC&R Research, 10 (4), pp. 393-420.

[17] Jaluria Y., 1980, "Natural Convection: Heat and Mass Transfer," Oxford, Pergamon Press.

[18] Aljuwayhel N.F., 2006, "Numerical and Experimental Study of the Influence of Frost Formation and Defrosting on the Performance of Industrial Evaporator Coils," PhD Thesis, University of Wisconsin-Madison.

[19] Voller V.R., and Prakash C., 1987, "A Fixed Grid Numerical Modeling Methodology for Convection-Diffusion Mushy Region Phase-Change Problems," Journal Heat and Mass Transfer, 30(8), pp. 1709-1719.

[20] Abdul Muttaleb Ali Al-Salman, 2005,"Numercal Investigation of Melting of Ice in a Box," Master Thesis, King Fahd University of Petroleum& Minerals.

[21] Roy S., Kumar H, Anderson R., 2005, "Efficient Defrosting of an Inclined Flat Surface," International Journal of Heat and Mass Transfer, 48, pp. 2613-2624.

Appendix A. Specifications of LCR Coil

Evaporator Coil

Model
LRC (5/8" tube)
610 x 2743 6r 4f 10c

Air		
Barometer	29.891	InchHg
Altitude	-0.114	ft
Airflow	10800	cfm
Velocity	600	fpm
On Coil	38.0/31.9	°F
Off Coil	32.0/28.4	°F
Cond Rate	0	g/s
Pressure drop	0.297	InchWg

Refrigerant (Evaporating R22)		
Temperature	25.0	°F
Abs. Press	63.3	Psi
Density	80.5	lb/ft³
Enthalpy Change	71.5	Btu/lb
Mass Flow	1040	lb/hr
dP Rate	0.00532	Psi/ft
Press Drop	0.561	Psi
Pipe Conn	1.38	inch

Performance		
Sensible Duty	74354	Btu/hr
Total Duty	74354	Btu/hr

DXC 1.2.1.0 registered to LRC Coil Co., Mike Williams

Appendix A. Specifications of LCR Coil (cont'd)

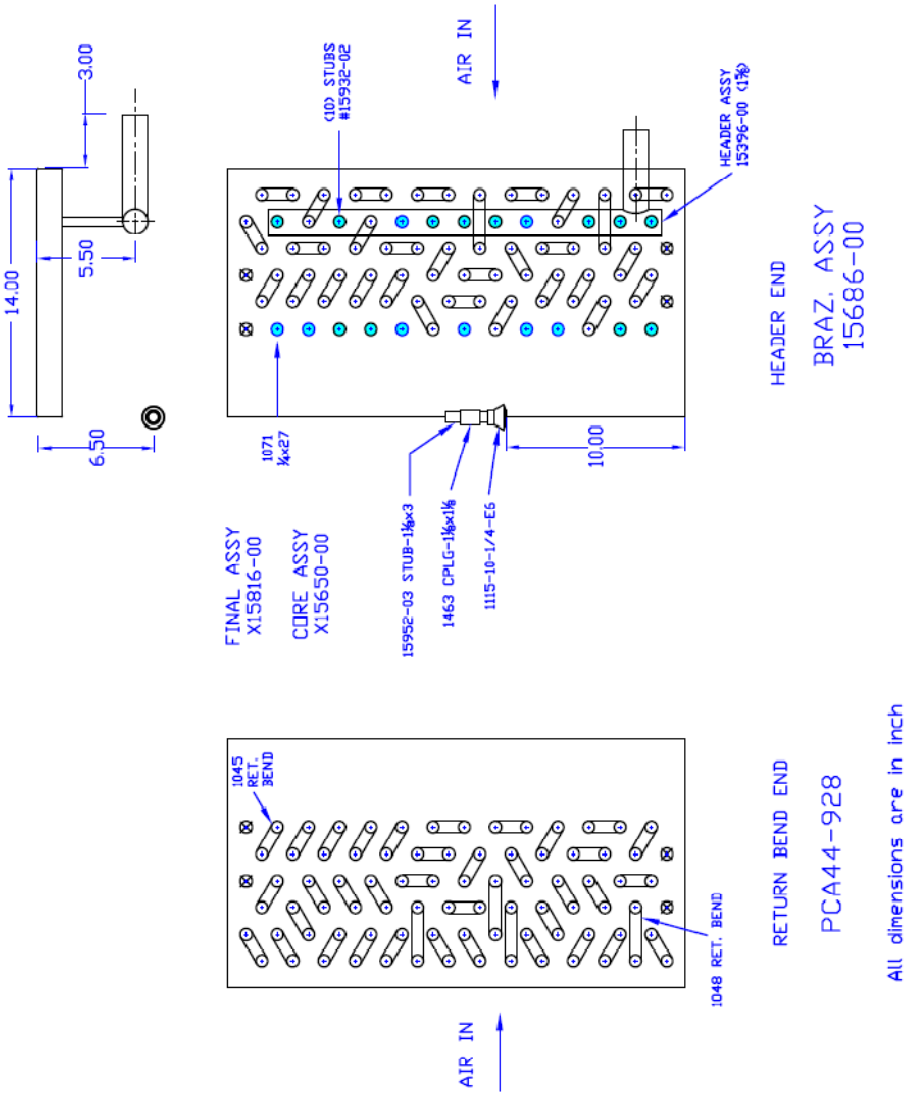

Appendix A. Specifications of LCR Coil (cont'd)

FIN DIMENSIONS

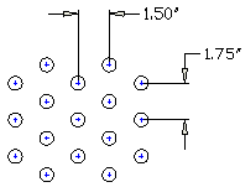

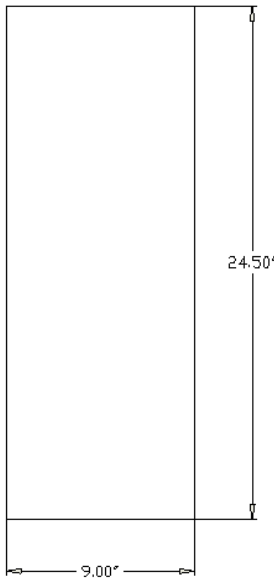

FIN LENGTH OF UNIT: 108"

EXPECTED STATIC PRESSURE DROP ON COIL: 0.297 IN H_2O

MOTOR RPM: 1040

Appendix B. User Defined Function (UDF) Code

```
/************************************************************/
/* This UDF is writen to calculate the evaporation rate     */
/* and energy at the free surface between frost surface     */
/* and air. This UDF will be inserted into phase interaction*/
/* in "phases" menu.
      */
/************************************************************/

#include "udf.h"
#include "sg.h"
#include "sg_mphase.h"
#include "flow.h"
#include "mem.h"
#include "metric.h"

/* USER INPUTS */

#define sigma 23.82e-3        /*surface tension coefficient of vapor-
liquid system, N/m*/
#define g 9.81                /* gravity, m/sec2 */
#define L_f 2501000           /* latent heat of evaporation, J/kg */
#define L_s 2834000           /* latent heat of sublimation, J/kg */
#define nu_a_am 1.2427e-5     /*kinematic viscosity of air at freezer
ambient temperature, m2/s*/
#define nu_w_am 1.24e-5       /*kinematic viscosity of water vapor,
m2/s*/
#define Rho_w_am 1.7426e-03   /*density of water vapor at freezer
ambient temperature T=258K,kg/m3*/
#define Rho_a_am 1.3678       /*density of dry air at freezer ambient
temperature T=258K,kg/m3*/
#define Rho_aw_am 1.36954     /*density of moist air at freezer ambient
temperature T=258K, kg/m3 */
#define mol_mass_w 18.01534   /* Molecular weight of water */
#define mol_mass_a 28.966     /* Molecular weight of air */
#define mu_w 1.34e-05
#define mu_a 1.7894e-05
#define P_am 101325           /* Ambient pressure, pascal */
#define T_am 258              /* Ambient temperature, K */
#define P_w_sat_am 192        /*  Saturated Water Pressure at freezer
temperature 258K and RH=80% is assumed constant, pascal */
#define fin_length 44.45e-3   /* Length of fin, m ; ~ 44.5mm */
#define Rel_Humid = 0.8       /* Relative Humidity in the freezer is
set at 80% */

/* END OF USER INPUTS */


/************************************************************/
/* UDF for specifying an interfacial area density           */
/************************************************************/

DEFINE_ADJUST(area_density, domain)
{
      Thread *t;
```

```
      Thread **pt;
      cell_t c;

      Domain *pDomain = DOMAIN_SUB_DOMAIN(domain,P_PHASE);
      {
            Alloc_Storage_Vars(pDomain,SV_VOF_RG,SV_VOF_G,SV_NULL);
            Scalar_Reconstruction(pDomain, SV_VOF,-1,SV_VOF_RG,NULL);
            Scalar_Derivatives(pDomain,SV_VOF,-
1,SV_VOF_G,SV_VOF_RG,Vof_Deriv_Accumulate);
      }
      mp_thread_loop_c (t,domain,pt)

      if (FLUID_THREAD_P(t))
      {
            Thread *tp = pt[P_PHASE];
            begin_c_loop (c,t)
            {
                  #if RP_3D
                      C_UDMI(c,t,0)
                      =sqrt(C_VOF_G(c,tp)[0]*C_VOF_G(c,tp)[0]+C_VOF_G(c,
                      tp)[1]*C_VOF_G(c,tp)[1]+C_VOF_G(c,tp)[2]*C_VOF_G(c
                      ,tp)[2]);
                  #endif

                  #if RP_2D
                      C_UDMI(c,t,0) =
                      sqrt(C_VOF_G(c,tp)[0]*C_VOF_G(c,tp)[0]+C_VOF_G(c,t
                      p)[1]*C_VOF_G(c,tp)[1]);
                  #endif
            }
            end_c_loop (c,t)
     }

 Free_Storage_Vars(pDomain,SV_VOF_RG,SV_VOF_G,SV_NULL);

}


DEFINE_MASS_TRANSFER(melted_vapor_source,c,thread,from_index,from_sps_i
ndex,to_index,to_sps_index)
{

      face_t f;
      real A[ND_ND],Del_Rho,Ave_Rho, nu_w,nu_a, m_w_s,area = 0.15e-
6,Rho_w_s, Rho_a, Rho_aw, P_w_sat_s;
      real Sh=0,Gr=0,Sc=0,Re,Nu,Pr,D_w2a, param, mass_transfer_coef,
heat_transfer_coef;
      real urel, urelx,urely,urelz, evap_rate=0., evap_rate2=0.,diam,
Q_evap, Q_convec, vof_grad, Q_sublime;

      Thread *frost = THREAD_SUB_THREAD(thread, from_index);
      /* Thread pointer to primary phase: frost phase */
      Thread *air = THREAD_SUB_THREAD(thread, to_index);
      /* Thread pointer to secondary phase: air phase */
      diam =  pow(C_VOLUME(c,frost), 1/3);
      urelx = C_U(c,air);
      urely = C_V(c,air);
```

```
urelz = C_W(c,air);
urel = sqrt(urelx*urelx + urely*urely + urelz*urelz);
/*relative velocity*/
vof_grad = C_UDMI(c,thread,0);
Re = urel * fin_length * C_R(c,air)/C_MU_L(c,air);
Pr = C_CP(c,air)*C_MU_L(c,air) / C_K_L(c,air);
Nu = 0.13*pow(Re, 0.5)*pow(Pr, 0.333);
/* This correlation is from Jaluria, 1980 */
heat_transfer_coef = Nu*C_K_L(c, air)/fin_length;
/* local heat transfer coefficient */

/* calculate mass transfer only where frost presents  */
if (C_VOF(c,frost)>0.1)
/* Assume evaporation happens when VOF of frost > 0.1 */
{
      if (C_T(c,frost)>273)
      {
           param = (C_T(c,frost)-273)*17.2694/(C_T(c,frost)-34.7);
           P_w_sat_s = exp(param);    /*Partial pressure of water
           vapor on frost surface, assume saturated    */
      }
      else
      {
           /* Use correlation by Murphy and Koop, 2005 */
           param = 9.550426 - 5723.265/C_T(c,frost)
           +3.53068*log(C_T(c,frost))-0.00728332* C_T(c,frost);
                        P_w_sat_s = exp(param);
           /* Partial pressure of water vapor on frost surface,
           assume saturated    */
           /*P_w_sat_s = exp(-6140.4/C_T(c,frost)+28.916); /*
           Partial pressure of water vapor */
      }

      Re = urel * diam * C_R(c,air)/C_MU_L(c,air);
      Pr = C_CP(c,air)*C_MU_L(c,air) / C_K_L(c,air);
      Nu = 0.13*pow(Re, 0.5)*pow(Pr, 0.333);
      /* This correlation is from Jaluria, 1980 */
      heat_transfer_coef = Nu*C_K_L(c, air)/diam;
      /* heat transfer coefficient */

      if (P_w_sat_s > P_w_sat_am)
      {

           /* Diffusion coef of water in to air. Use correlation of
           Bolz and Tuve 1976 */
           D_w2a = -2.775e-6 + (4.478e-8)*C_T(c,frost) + (1.656e-
           10)*pow(C_T(c,frost), 2); /* Unit, m2/s */

           Rho_w_s = P_w_sat_s*mol_mass_w)/(UNIVERSAL_GAS_CONSTANT*
           C_T(c, frost));

           /* Density of water vapor at the frost surface */
           Rho_a = C_R(c,air);
           /* Density of air at the frost surface */
           Rho_aw = Rho_w_s + Rho_a;

           /* Density of moist air at the frost surface */
```

```
                Del_Rho = abs(Rho_aw_am - Rho_aw);
                /* Difference of Moist Air Density */
                Ave_Rho = (Rho_aw_am + Rho_aw)/2;
                /* Average density  */
                nu_w = mu_w/Rho_w_s;
                nu_a = C_MU_L(c,air)/C_R(c,air);
                Sc = nu_a/D_w2a;

                /* Grass Holf Number */
                Gr = ((Del_Rho/Ave_Rho)*g*pow(diam,3))/(nu_a*nu_a);
                /* For heat transfer coefficient, use Sh instead of Nu*/
                Sh =  0.13*pow(Gr*Sc,1/3) ;


                mass_transfer_coef = D_w2a*Sh/diam; /* Unit m/s */

                /* rate of evaporation */
                evap_rate = mass_transfer_coef*(Rho_w_s -
                Rho_w_am)*C_VOF(c,frost)*C_UDMI(c,thread,0);
                /* Unit, kg/m3.s as per Fluent procedure*/
                evap_rate2 = mass_transfer_coef*(Rho_w_s - Rho_w_am);
                Q_evap = evap_rate*L_f;
                Q_sublime = evap_rate*L_s;

            }
            else
            {
                evap_rate= 0;
            }
      }
      return 2*evap_rate;
}


DEFINE_SOURCE(energy, cell, thread, dS, eqn)
{
      real x[ND_ND];
      real source;
      Thread *tm = thread;
      source = C_UDMI(cell, tm, 3);
      dS[eqn] = 0;

  return source;
}
```

Appendix C. CFD Modeling Overview of Hot Gas Defrost Problem